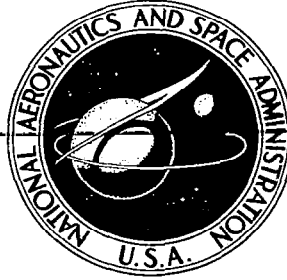


**NASA CONTRACTOR
REPORT**



NASA CR-2

0061696



TECH LIBRARY KAFB, NM

NASA CR-2823

LOAN COPY: RETURN TO
AFWL TECHNICAL LIBRARY
KIRTLAND AFB, N. M.

**ROOM-TEMPERATURE-OPERATION
VISIBLE-EMISSION SEMICONDUCTOR
DIODE LASERS**

I. Ladany, H. Kressel, and C. J. Nuese

Prepared by
RCA LABORATORIES
Princeton, N.J. 08540
for Langley Research Center

NATIONAL AERONAUTICS AND SPACE ADMINISTRATION • WASHINGTON, D. C. • APRIL 1977



0061696

1. Report No. NASA CR-2823		2. Government Accession No.		3. Recipient's Catalog No.	
4. Title and Subtitle ROOM-TEMPERATURE-OPERATION VISIBLE-EMISSION SEMICONDUCTOR DIODE LASERS				5. Report Date April 1977	
7. Author(s) I. Ladany, H. Kressel, and C. J. Nuese				6. Performing Organization Code	
9. Performing Organization Name and Address RCA Laboratories Princeton, New Jersey 08540				8. Performing Organization Report No. PRRL-76-CR-16	
12. Sponsoring Agency Name and Address Langley Research Center National Aeronautics & Space Administration Hampton, VA 23665				10. Work Unit No.	
				11. Contract or Grant No. NAS1-13739	
15. Supplementary Notes Langley Technical Monitor: Herbert D. Hendricks Final Report				13. Type of Report and Period Covered Contractor Report (2-12-75 to 2-11-76)	
				14. Sponsoring Agency Code	
16. Abstract <p>Two main approaches were taken to develop shorter wavelength semiconductor lasers. (1) Based on (AlGa)As and liquid-phase epitaxy, significant new results were obtained: Reductions in J_{th} by a factor of at least 2 were achieved down to 7240 A, as was room-temperature cw operation for the first time at 7400 A. Properties of these laser diodes (power output, spectra, and beam patterns), materials considerations, laser theory, and growth problems are discussed. Hall data and PL measurements for high Al containing layers are reported. The design of (AlGa)As layers is discussed from the vertical point of view (i.e., the requirements imposed on cavity dimensions, Al content of the layers, etc.) and various design curves are given. Horizontal structural requirements, principally the effect of edge leakage on the stripe-geometry laser threshold current, are also discussed. Experimental results from measurements done as a function of hydrostatic pressure are correlated with other results. (2) The first heterojunction laser structures using $\text{GaAs}_{1-x}\text{P}_x$ and $\text{In}_y\text{Ga}_{1-y}\text{P}$ at compositions, where the lattice constants are matched, were grown using vapor-phase growth technology and are described in detail, including experimental device results. Threshold current densities from 3000 to 5000 A/cm^2 and emission wavelengths from 6520 A to 6640 A were obtained at 77 K. However, optical confinement was effective up to at least 273 K, as the threshold current density increased by no more than a factor of 10 in raising the temperature to that value from 77 K. The limiting factor in these devices is nonradiative recombination at the heterojunctions. Life tests on facet-coated (AlGa)As cw diodes are reported. Coated units have accumulated 10,000 hours of continuous operation, and uncoated lasers have passed 14,000 hours with some increase in threshold current due to facet erosion.</p>					
17. Key Words (Selected by Author(s)) Semiconductors Semiconductor diodes (AlGa)As lasers Vapor-phase growth Heterojunction laser structures			18. Distribution Statement Unclassified- Unlimited Subject Category 76		
19. Security Classif. (of this report) Unclassified		20. Security Classif. (of this page)		21. No. of Pages 67	22. Price* \$4.50

*For sale by The National Information Service, Springfield, Virginia 22151



TABLE OF CONTENTS

Section	Page
SUMMARY	1
I. INTRODUCTION	3
II. (AlGa)As LASERS	4
A. Introduction	4
B. Materials Growth and Properties	5
C. Laser Design Considerations	15
1. Vertical Laser Structure	15
2. Horizontal Design Considerations	20
D. Experimental Laser Results	26
III. VAPOR-PHASE GROWTH OF GaAs _{1-x} P _x /In _y Ga _{1-y} P HETEROJUNCTION LASER STRUCTURES	34
A. Lattice Matching GaAs _{1-x} P _x with In _y Ga _{1-y} P	34
B. Vapor-Phase Growth	36
C. Structure	37
D. Laser Properties	39
IV. RELIABILITY STUDIES	45
V. CONCLUSIONS	49
APPENDIX A - Reliability Aspects and Facet Damage in High-Power Emission from (AlGa)As CW Laser Diodes at Room Temperature	51
REFERENCES	61



LIST OF ILLUSTRATIONS

Figure	Page
1. Relative visibility of devices emitting at various wavelengths with constant beam width, source size, and power emission	4
2. Carrier concentration and mobility as a function of x, the mole fraction of Al in $\text{Al}_x\text{Ga}_{1-x}\text{As}$. The dopant concentration in the melt was 0.64 At. % for Ge and 0.7 At. % for the single Zn sample	6
3. Photomicrograph of beveled and stained DH structure. The magnification along the layers is 95X and normal to the layers, 5400X	7
4. Photomicrographs of beveled and stained high-threshold DH laser structure. Magnification is the same as in Fig. 3	8
5. Bandgap energy of $\text{Al}_x\text{Ga}_{1-x}\text{As}$ as determined by microprobe measurements and photoluminescence	9
6. Lasing wavelength and photon energy in $\text{Al}_x\text{Ga}_{1-x}\text{As}$ (undoped recombination region); $h\nu = E_g - 0.03 \text{ eV}$	11
7. Refractive index step at $\text{Al}_x\text{Ga}_{1-x}\text{As}/\text{GaAs}$ heterojunction ($\lambda \cong 9000 \text{ \AA}$). Line A is from Ref. 6 and line B is from Ref. 5	12
8. Photoluminescence at 77 K of $\text{Al}_{.48}\text{Ga}_{.52}\text{As}:\text{Ge}$ and Zn ($4416\text{-}\overset{\circ}{\text{A}}$ laser excitation)	13
9. Ionization energy of Ge in $(\text{AlGa})\text{As}$ as a function of Al and of Zn at $\text{Al}_{.47}\text{Ga}_{.52}\text{As}$	14
10. Theoretical radiation confinement factor Γ as a function of cavity width (J. K. Butler, unpublished)	17
11. Theoretical dependence of J_{th} on the heterojunction spacing, d	18
12. Calculated internal quantum efficiency as a function x, the mole fraction of Al in $(\text{AlGa})\text{As}$, and the lasing wavelength	21
13. Leakage current at edges of stripe laser	22
14. Sheet resistivity measurement	24
15. J_S/J_∞ for a number of diodes made from different wafers. A plot of Eq. (19) with $W = 13 \text{ }\mu\text{m}$ and $J_\infty = 2000 \text{ A/cm}^2$ is also shown	25

LIST OF ILLUSTRATIONS (Continued)

Section	Page
16. Cross section (not to scale) of low-threshold laser diodes with $x \lesssim 0.2$	26
17. Performance characteristics of laser diode operating cw at room temperature. (a) Power output, one side, as a function of current. (b) Spectral emission at 450 mA (6 mW of power emitted). (c) Far-field pattern in the direction perpendicular to the junction plane	29
18. Room-temperature threshold current densities of DH (AlGa)As laser diodes vs emission wavelength. This work is compared with the lowest J_{th} values reported in the literature . . .	31
19. Comparison of experimental data and theory on the hydrostatic pressure dependence of the threshold current density of (AlGa)As lasers (work of Y. Juravel and P. M. Raccah, Yeshiva University)	33
20. Room-temperature energy-bandgap values of $In_{1-y}Ga_yP$ and $GaAs_{1-x}P_x$ alloys for lattice-matched structures of $In_{1-y}Ga_yP/GaAs_{1-x}P_x$	35
21. Schematic diagram of the vapor-phase growth system used for the epitaxial deposition of single-crystalline layers of $In_yGa_{1-y}P$ and $GaAs_{1-x}P_x$	36
22. Schematic presentation of vapor-grown $GaAs_{1-x}P_y/In_yGa_{1-y}P$ heterojunction structure prepared for visible-light-emitting laser diodes	38
23. Threshold current dependence of heterojunction laser (InGaP/GaAsP)	40
24. Shift of emission lines as a function of current as lasing is approached at 77 K	42
25. Light output as a function of the diode current of a GaAsP/InGaP heterojunction diode and of an (AlGa)As/GaAs DH device. The nonlinearity of the diode indicates the presence of strong nonradiative current components due to defects in the GaAsP/InGaP diode	43
26. Experiment showing the effect of a lattice parameter mismatch on the relative efficiency of a DH LED of $In_xGa_{1-x}P/GaAs$. The efficiency scale is in arbitrary units, but the two curves can be compared. A mismatch of 0.6% produces a severe reduction in the diode efficiency, and the light output is a steeper function of the diode current, indicating a larger nonradiative current contribution	44

LIST OF ILLUSTRATIONS (Continued)

Section	Page
27. Power output as a function of current (cw) of a 13- μm -wide stripe laser made using the fast-cool Zn-doped process, before and after constant current operation . .	46
28. Laser facet following catastrophic degradation. Only the uncoated regions show facet damage, while the coated central region shows no evidence of such damage	47
29. Power output as a function of current (cw) of a wide stripe laser during operation. For the first 9000 h, the laser was operated at 0.8 A; after that at 0.9 A	48

ROOM-TEMPERATURE-OPERATION VISIBLE-EMISSION
SEMICONDUCTOR DIODE LASERS

by

I. Ladany, H. Kressel, and C. J. Nuese

RCA Laboratories
Princeton, New Jersey 08540

SUMMARY

Two main approaches have been taken in a program aimed at developing shorter wavelength semiconductor lasers. In the first, based on (AlGa)As and liquid-phase epitaxy, significant new results have been obtained. Important reductions in threshold current density (a factor of at least 2 lower than previously reported) were obtained down to 7240 \AA , and room temperature cw operation was achieved for the first time at 7400 \AA , a wavelength in the convenient viewing range. Properties of these laser diodes including power output, spectra, and beam patterns are reported. Materials considerations, laser theory, and growth problems are discussed, and Hall data and PL measurements for high Al containing layers are reported. The design of (AlGa)As layers is discussed from the vertical point of view (i.e., the requirements imposed on cavity dimensions, Al content of the layers, etc.), and various design curves are given. Horizontal structural requirements, principally the effect of edge leakage on the stripe threshold current, are also discussed. Experimental results obtained from measurements performed as a function of hydrostatic pressure are correlated with other results.

In the second approach, the first heterojunction laser structures using $\text{GaAs}_{1-x}\text{P}_x$ and $\text{InGa}_{1-y}\text{P}_y$ at compositions where the lattice constants are matched were grown using vapor-phase growth technology. The compositions for lattice matching are given, and the vapor phase process used is described in detail, including experimental device results. Threshold current densities in the range of 3000 to 5000 A/cm^2 and

emission wavelengths from 6520 Å to 6640 Å have been obtained at 77 K. However, optical confinement was effective up to at least 273 K, as the threshold current density increased by no more than a factor of 10 in raising the temperature to that value from 77 K. The limiting factor in these devices is deduced to be nonradiative recombination at the heterojunctions.

Life tests on (AlGa)As cw diodes are reported, and the effect of facet coating discussed. Coated units have accumulated 10,000 hours of continuous operation, and uncoated lasers have passed 14,000 hours with some increase in threshold current due to facet erosion.

I. INTRODUCTION

The present program was addressed to the development of shorter-wavelength room-temperature lasers than previously available, with the requirement of a reasonable operating life so that practical applications of these devices could be made. As the reduction in the wavelength generally implies an increase in the threshold current density, efforts were made to reduce the current requirement of stripe lasers by materials improvement and technological developments.

Need for shorter-wavelength lasers generally falls into two categories: (1) If the visibility is increased, various applications depending on the eye response become possible, and (2) the shorter wavelength leads to improved high-speed film data encoding, and other instrumental applications requiring well-focused, high-intensity spots, a task eased by reducing the wavelength.

The work done in the course of this program has led to several important advances. The lowest recorded threshold current densities were obtained in the 7000- to 8000-Å spectral range and cw operation was obtained at room temperature for the first time at 7400 Å, with the emission of several milliwatts of power. These advances were made possible by improved growth procedures using liquid-phase epitaxy, and improved understanding concerning the role of dopants, and their incorporation in (AlGa)As. In addition, experiments were begun in producing heterojunction structures by vapor-phase epitaxy using the GaAsP/InGaP lattice matched combinations. Lasing was obtained with these structures, although not yet at room temperature.

II. (AlGa)As LASERS

A. Introduction

For a given power output, the visibility of devices in the 7000- to 8000-Å range is a steep function of the emission wavelength, as shown in Fig. 1. Thus, great increases in visibility can be achieved from even

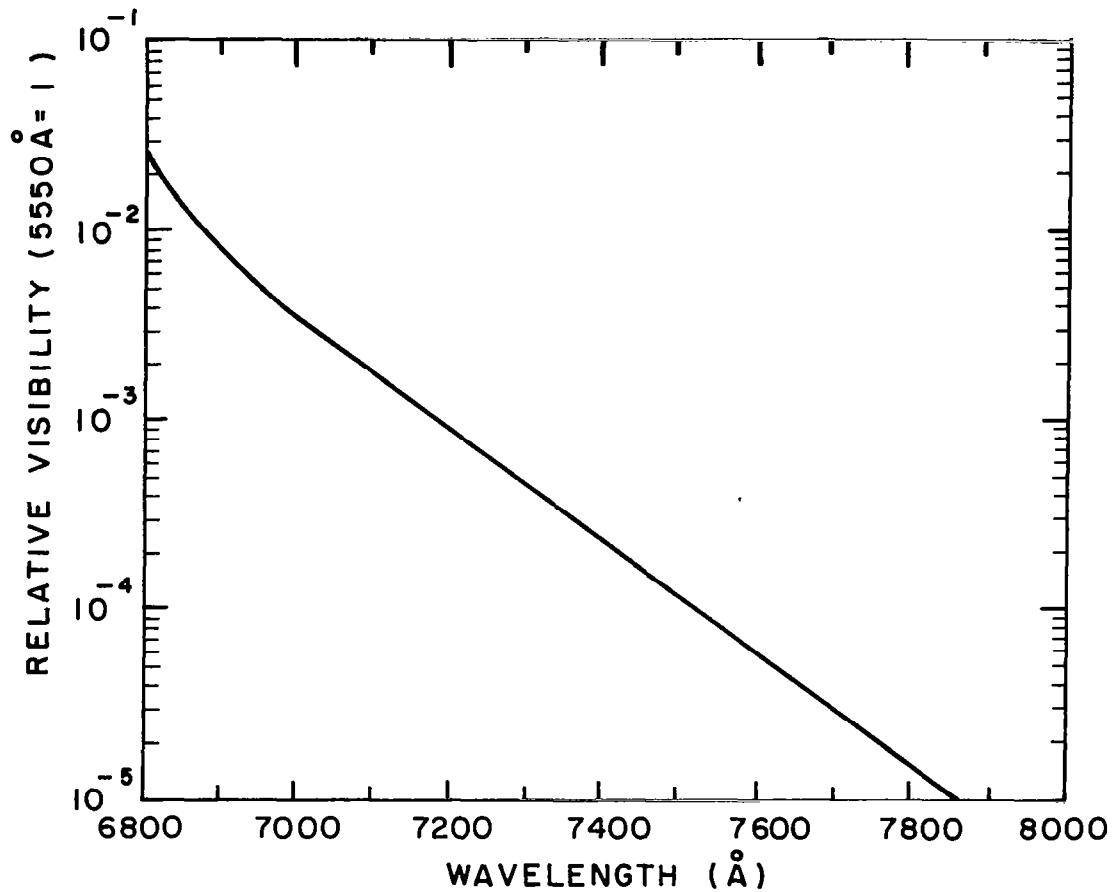


Figure 1. Relative visibility of devices emitting at various wavelengths with constant beam width, source size, and power emission.

modest shifts in wavelength toward 7000 Å. This section covers design aspects, materials considerations, and major experimental results obtained

from our efforts to shift the emission wavelength while maintaining room-temperature operating conditions, and includes discussions of our record-low J_{th} values and our short-wavelength room-temperature laser diode.

B. Materials Growth and Properties

Procedures used in growing the layers were generally those described in the previous report (Ref. 1). However, the high aluminum content of the confining layers caused problems in the use of tin and germanium dopants which are preferred in the case of infrared emitting lasers. Better results were obtained using Te as the n-type dopant and zinc as the p-type dopant. In the case of tin we attribute our difficulties to the very low segregation coefficient, requiring tin concentrations in the melt which may interfere with the uniform growth of (AlGa)As layers. The use of germanium as the p-dopant in high aluminum layers leads to more serious difficulties. To study this problem, several layers of (AlGa)As were grown under conditions similar to those prevailing during laser material growth.

The substrates for these runs were chromium-doped GaAs samples, and great care was taken to avoid contaminating the grown layer with chromium from dissolved portions of the substrate. As a consequence, the interface between the substrate and the grown layer was not always planar, making the thickness of the layer somewhat variable. Measurements were made at room temperature, using the Van der Pauw method, by alloying gold-zinc contacts into four corners of rectangular samples. The aluminum content of the layers was determined by electron microprobe, and the layers were also studied by photoluminescence. Carrier concentration and mobility values are given in Fig. 2, together with published data for lower x values. It can be seen that with increasing aluminum content in the grown layer, the mobility and carrier concentrations of the doped layers decrease and, consequently, the resistivity increases. With zinc as the p-dopant, the mobility is about that of p-type GaAs, and the resistivity

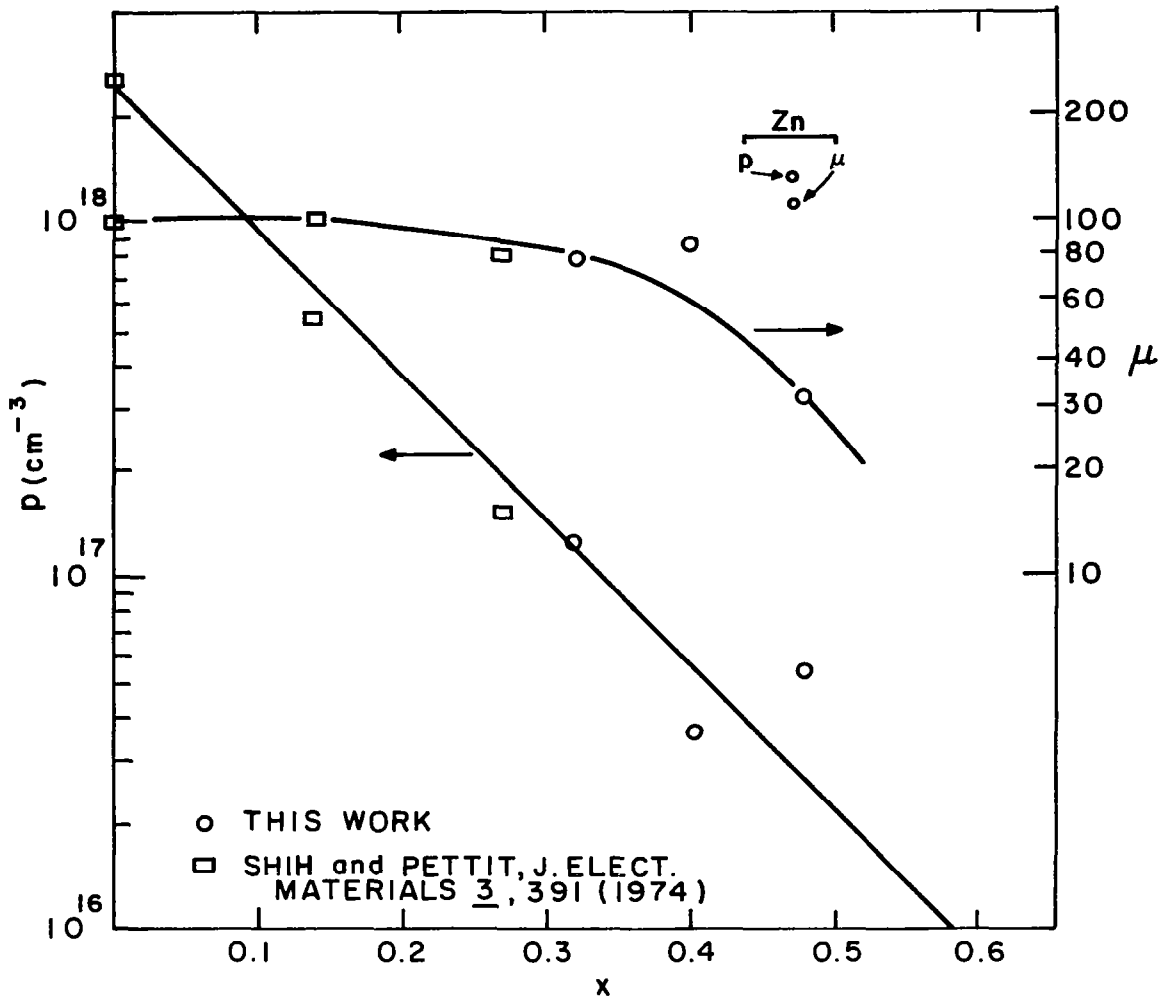


Figure 2. Carrier concentration and mobility as a function of x , the mole fraction of Al in $\text{Al}_x\text{Ga}_{1-x}\text{As}$. The dopant concentration in the melt was 0.64 At. % for Ge and 0.7 At. % for the single Zn sample.

drops by almost a factor of 100 for roughly the same zinc concentration in the melt. It is clear that zinc-doped high aluminum layers will have a significantly lower resistance, and thus contribute to improved cw operation.

A convenient way of studying the structural perfection of the layers is to bevel them to a small angle, typically 1 deg. When such a beveled edge is stained and photographed under a modest magnification, one obtains a greatly expanded picture of the structure in a direction normal to the layers, and a relatively compressed picture in a direction along the interfaces. Thus, fairly long regions of the wafer can be examined in detail. Figures 3 and 4 show such photomicrographs, where the magnification is $\sim 5400X$ in one direction, and $95X$ in the other. The excellent

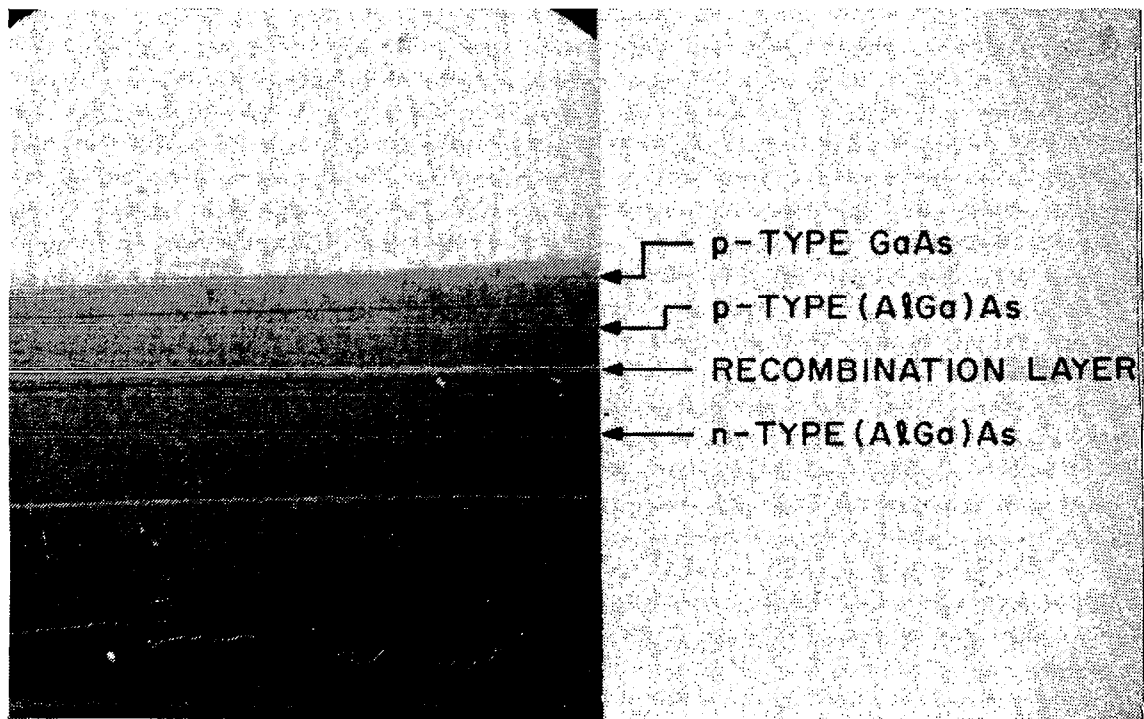


Figure 3. Photomicrograph of beveled and stained DH structure. The magnification along the layers is $95X$ and normal to the layers, $5400X$.

planarity of the layers and interfaces in Fig. 3 can be contrasted to that shown in Fig. 4, which was obtained from a high threshold wafer where

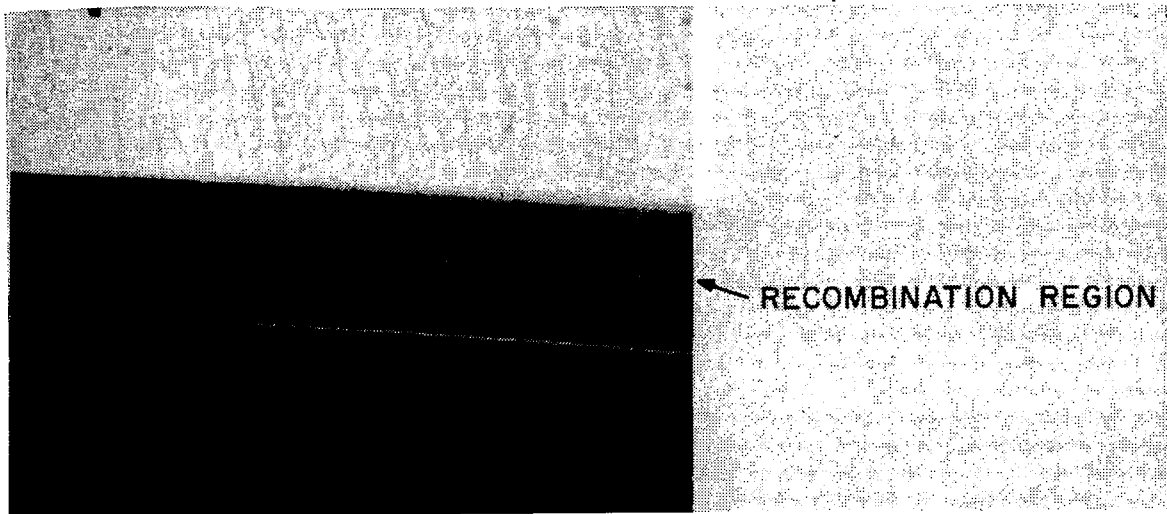


Figure 4. Photomicrograph of beveled and stained high-threshold DH laser structure. Magnification is the same as in Fig. 3.

a disturbance in the growth resulted in the staircase appearance of the recombination layer. It is tempting to associate the surface contour lines with these steps, but as shown in Fig. 3 this is not always the case. A disturbance of the magnitude shown in Fig. 4 always increases the threshold, but smaller fluctuations, contrary to expectations, do not correlate with increases in threshold current density.

The aluminum concentrations in the relevant regions of the laser were determined by electron microprobe analysis, except for the recombination region which is too thin for this measurement and where the aluminum concentration was estimated from the emission wavelength.

Figure 5 shows the dependence of the bandgap energy as experimentally determined by electron microprobe measurements and photoluminescence as a function of aluminum concentration. The X minima (six equivalent valleys) are $\Delta E = 0.38$ eV (Ref. 2) above the Γ minimum of 1.424 eV. The experimental data for the Γ minimum follows the expression

$$E_{g\Gamma} = 1.424 + 1.266x + 0.266x^2 \quad (1)$$

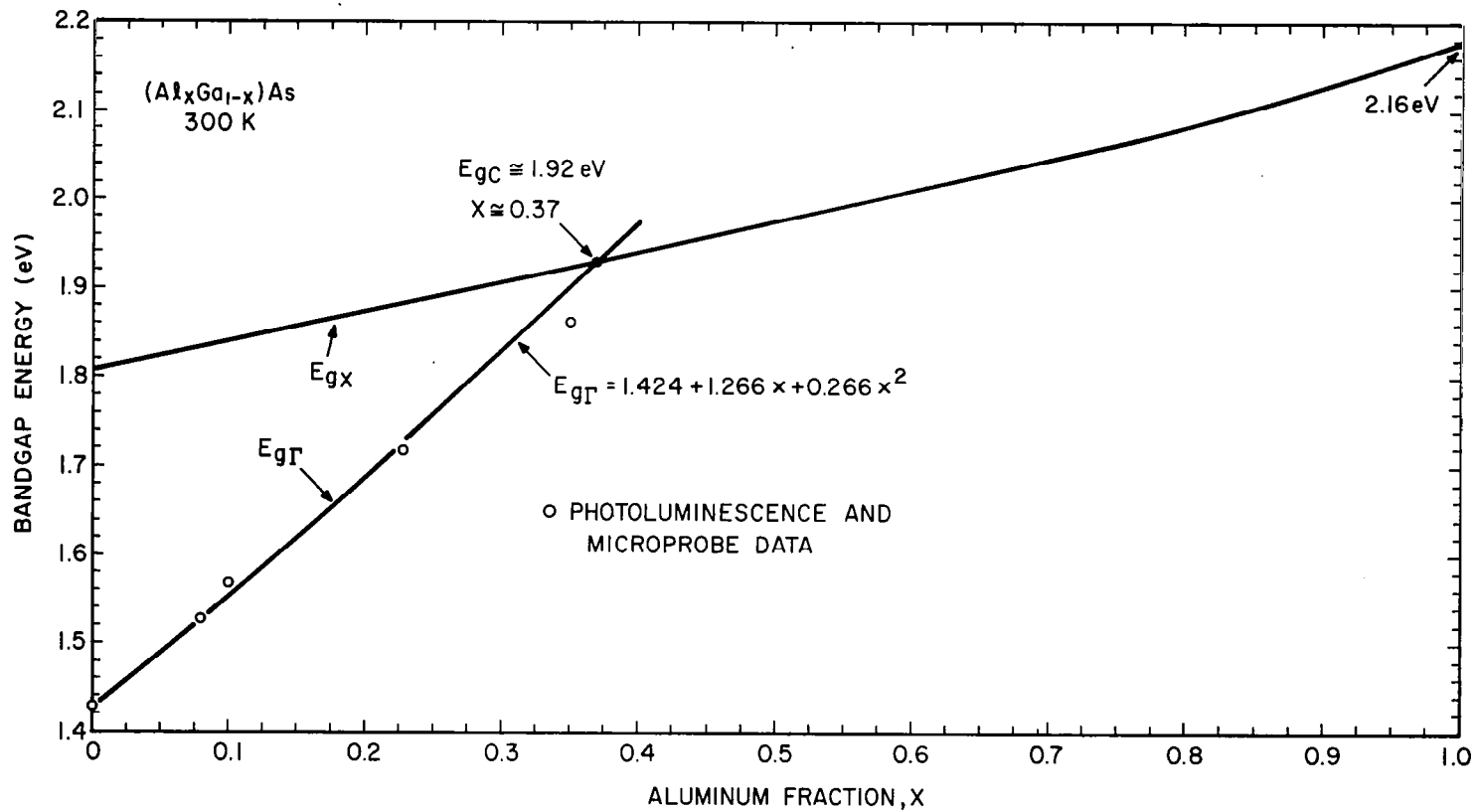


Figure 5. Bandgap energy of Al_xGa_{1-x}As as determined by microprobe measurements and photoluminescence.

in agreement with electroreflectance data (Ref. 3).

The lasing photon energy in undoped GaAs is 20 to 30 meV below the bandgap energy (Ref. 4). Assuming that this relationship holds (as it should since the lower lasing photon energy is due to the injected plasma effect), then using a value of $E_g - h\nu = 30$ meV,

$$h\nu_L = 1.394 + 1.266x + 0.266x^2 \quad (2)$$

which is plotted in Fig. 6.

The refractive index values used to determine the mode-guiding properties of the lasers can be deduced from the plot shown in Fig. 7. The values plotted are the refractive index at about $0.9 \mu\text{m}$ as determined by direct measurement (Ref. 5) and as deduced from the mode-guiding properties of heterojunction laser diodes with GaAs in the recombination region (Ref. 6). At the lasing wavelength, the refractive index remains at 3.59 to 3.60 throughout the direct bandgap region of (AlGa)As (Ref. 5). Therefore, the refractive index step Δn of lasers with differing aluminum concentrations Δx in the recombination region can be quite well approximated by assuming that

$$\Delta n \approx 0.62\Delta x \quad (3)$$

Note, however, that differing free carrier concentrations on the two sides of the heterojunction boundary affect the refractive index step, although this effect is small ($\Delta n \approx 0.1$) under likely circumstances.

The effective ionization energy of germanium in the high aluminum concentration range of the alloy was determined by photoluminescence and compared with values obtained using zinc. Figure 8 shows the photoluminescence spectrum of $\text{Al}_{.47}\text{Ga}_{.53}\text{As}$ Zn-doped sample and of a Ge-doped $\text{Al}_{.48}\text{Ga}_{.52}\text{As}$ sample. The emission peak in both samples is due to the acceptor, with the bandgap luminescence not being observable (a common feature in indirect bandgap materials). The bandgap energy at 77 K for this material is estimated to be 2.05 eV, and the peak of the Zn-doped sample is ≈ 0.08 eV below E_g , while for the Ge-doped sample the peak is

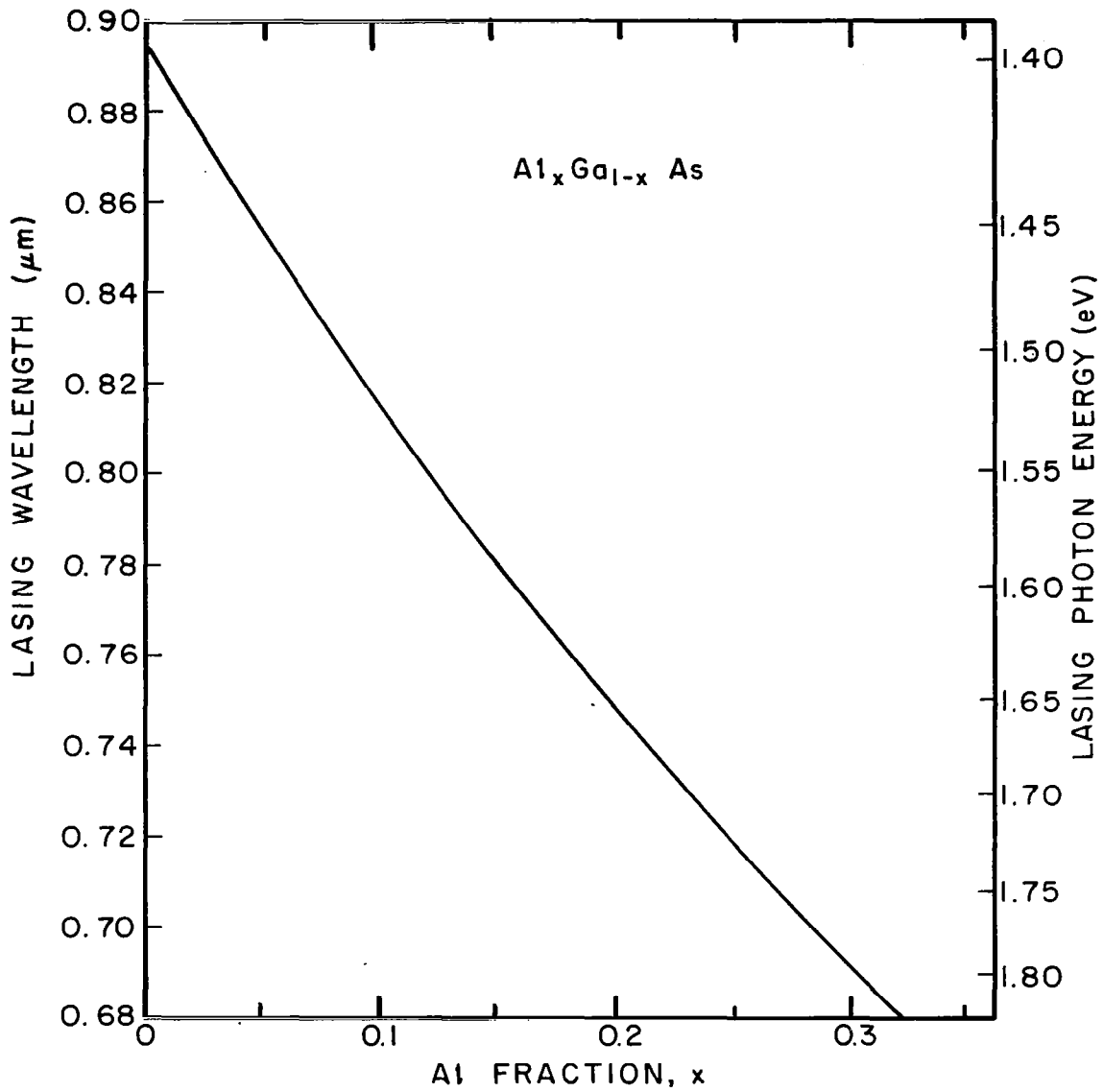


Figure 6. Lasing wavelength and photon energy in $\text{Al}_x\text{Ga}_{1-x}\text{As}$ (undoped recombination region); $h\nu = E_g - 0.03 \text{ eV}$.

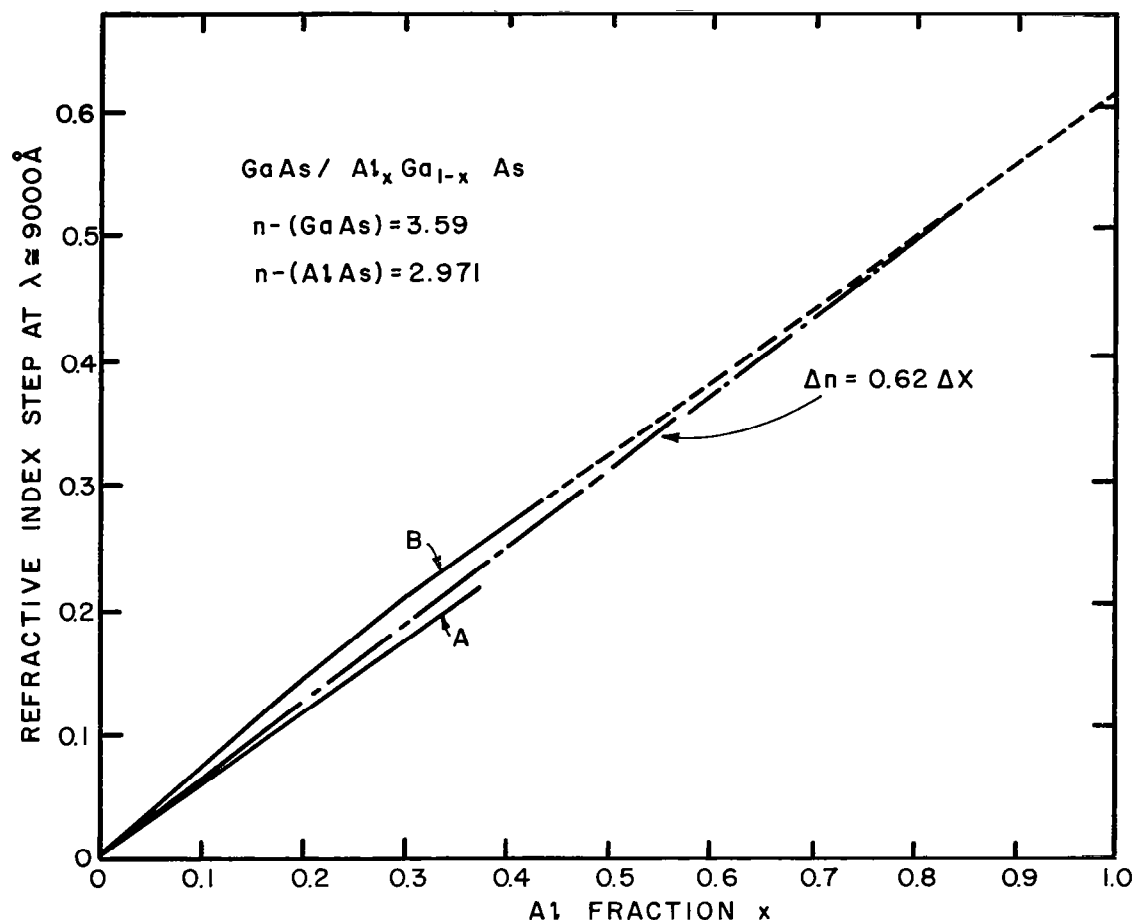


Figure 7. Refractive index step at $\text{Al}_x\text{Ga}_{1-x}\text{As}/\text{GaAs}$ heterojunction ($\lambda \approx 9000 \text{ \AA}$). Line A is from Ref. 6 and line B is from Ref. 5.

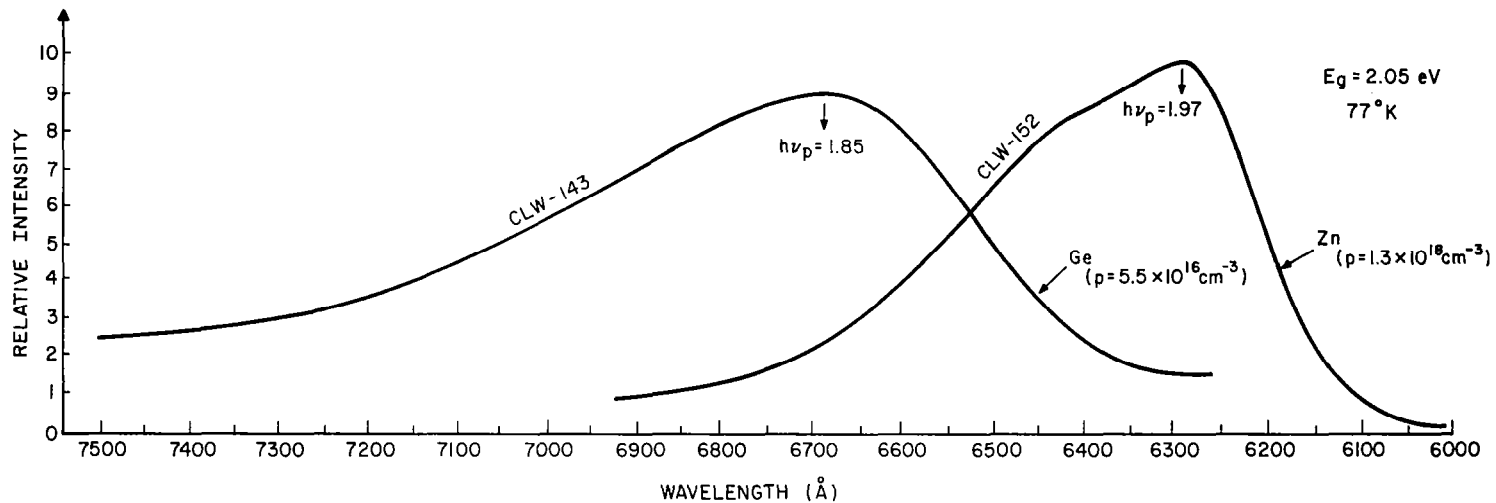


Figure 8. Photoluminescence at 77 K of Al_{0.48}Ga_{0.52}As:Ge and Zn (4416-Å laser excitation).

~ 0.2 eV below E_g , reflecting the much larger ionization energy of germanium. Figure 9 shows the present data added to our earlier measurements, which were limited to lower aluminum concentrations ($x \lesssim 0.4$). It is clear that the "effective" ionization energy of the germanium acceptor increases with aluminum concentration, particularly in the vicinity of the direct-to-indirect bandgap crossover composition at $x \sim 0.37$.

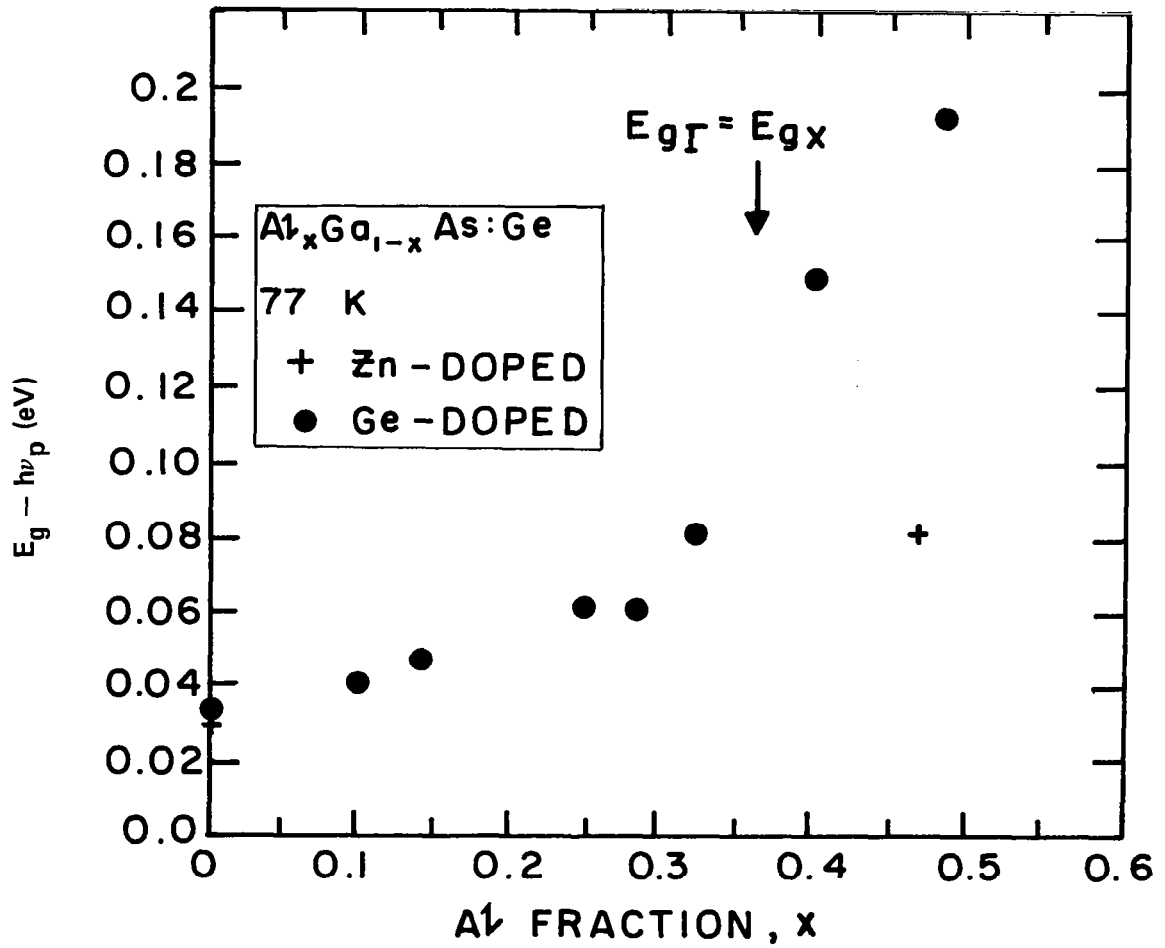


Figure 9. Ionization energy of Ge in (AlGa)As as a function of Al and of Zn at $Al_{.47}Ga_{.53}As$.

C. Laser Design Considerations

1. Vertical Laser Structure. - The dependence of J_{th} on cavity dimensions and refractive index step may be calculated, knowing the relationship between the gain coefficient of the recombination region and the diode current density. For undoped GaAs, the gain coefficient in the range 30 to 100 cm^{-1} is approximated by the theoretical relation (Ref. 7)

$$g = \beta(J_{nom} - J_1) \quad (4)$$

where

$$J_{nom} = \eta_i \frac{J}{d} \quad (5)$$

and J_1 and β are temperature-dependent quantities. At 300 K, $\beta = 0.044$ cm/A and $J_1 = 4100$ A/cm^2 .

The gain coefficient g_{th} of the recombination region at threshold is deduced from the lasing condition.

$$\Gamma(g_{th} - \alpha_{fc}) = \alpha_{end} + (1 - \Gamma)\alpha_{out} \quad (6)$$

Here, Γ is the fraction of the propagating power that lies within the recombination region. α_{end} is the Fabry-Perot cavity-end loss, α_{fc} is the free carrier absorption coefficient within the recombination region, and α_{out} is the absorption coefficient in the (AlGa)As bounding regions (assumed equal for the n- and p-type regions). Equal wave spreading into each of the two bounding regions is also assumed. From Eq. (6), we obtain

$$g_{th} = \frac{1}{\Gamma} \alpha_{end} + \frac{(1-\Gamma)}{\Gamma} \alpha_{out} + \alpha_{fc} \quad (7)$$

Rewriting Eq. (7) in terms of g_{th} and J_{th} ,

$$J_{th} = \frac{d}{\eta_i} \left(\frac{g_{th}}{\beta} + J_1 \right) \quad (8)$$

To calculate J_{th} we need to determine g_{th} and Γ . Considering first g_{th} , the determination of Γ is from Fig. 10*; the cavity-end loss is determined from the measured laser diode length L ; the absorption coefficient values involve some uncertainty since they must be deduced indirectly. A value of 10 cm^{-1} is experimentally justified for α_{fc} (Ref. 8). The absorption coefficient outside of the recombination region, estimated from the doping level in the n- and p-type (AlGa)As bounding layers, is $\alpha_{out} \sim 10 \text{ cm}^{-1}$ at room temperature. Therefore,

$$g_{th} = \frac{1}{\Gamma} \left(\frac{1}{L} \ln \frac{1}{R} + 10 \right); \text{ with } L = 500 \text{ } \mu\text{m}, g_{th} = 33/\Gamma \text{ cm}^{-1}.$$

Hence, from Eq. (8)

$$J_{th} = \frac{d}{\eta_i} \left(\frac{33}{\Gamma\beta} + J_1 \right) \quad (9)$$

The theoretical dependence of J_{th} on d in GaAs (for an assumed η_i value) for a given heterojunction barrier height can now be calculated since all of the needed parameters have been established. Figure 11 shows the calculated curves from Eq. (9) for several values of Δn . For large d values (approaching $1 \text{ } \mu\text{m}$) the theoretical curve yields $J_{th}/d = 4846 \text{ A/cm}^2 \mu\text{m}$. For small d values, the minimum J_{th} value is achieved at differing d values for various Δn . With $\Delta n = 0.4$, the lowest $J_{th} = 475 \text{ A/cm}^2$ is calculated at $d = 0.06 \text{ } \mu\text{m}$, and has, in fact, been achieved in GaAs/Al_{0.6}Ga_{0.4}As DH lasers with $d \approx 0.1 \text{ } \mu\text{m}$ (Ref. 9). For smaller Δn values, the minimum calculated J_{th} is increased and occurs at larger d values because the radiation confinement decreases with decreasing d , leading to large increases in the required recombination region gain coefficient at threshold. The experimental points in Fig. 11 were obtained from lasers where $x \approx 0.1$ in the recombination region and are in approximate agreement with calculations.

*J. K. Butler, unpublished work.

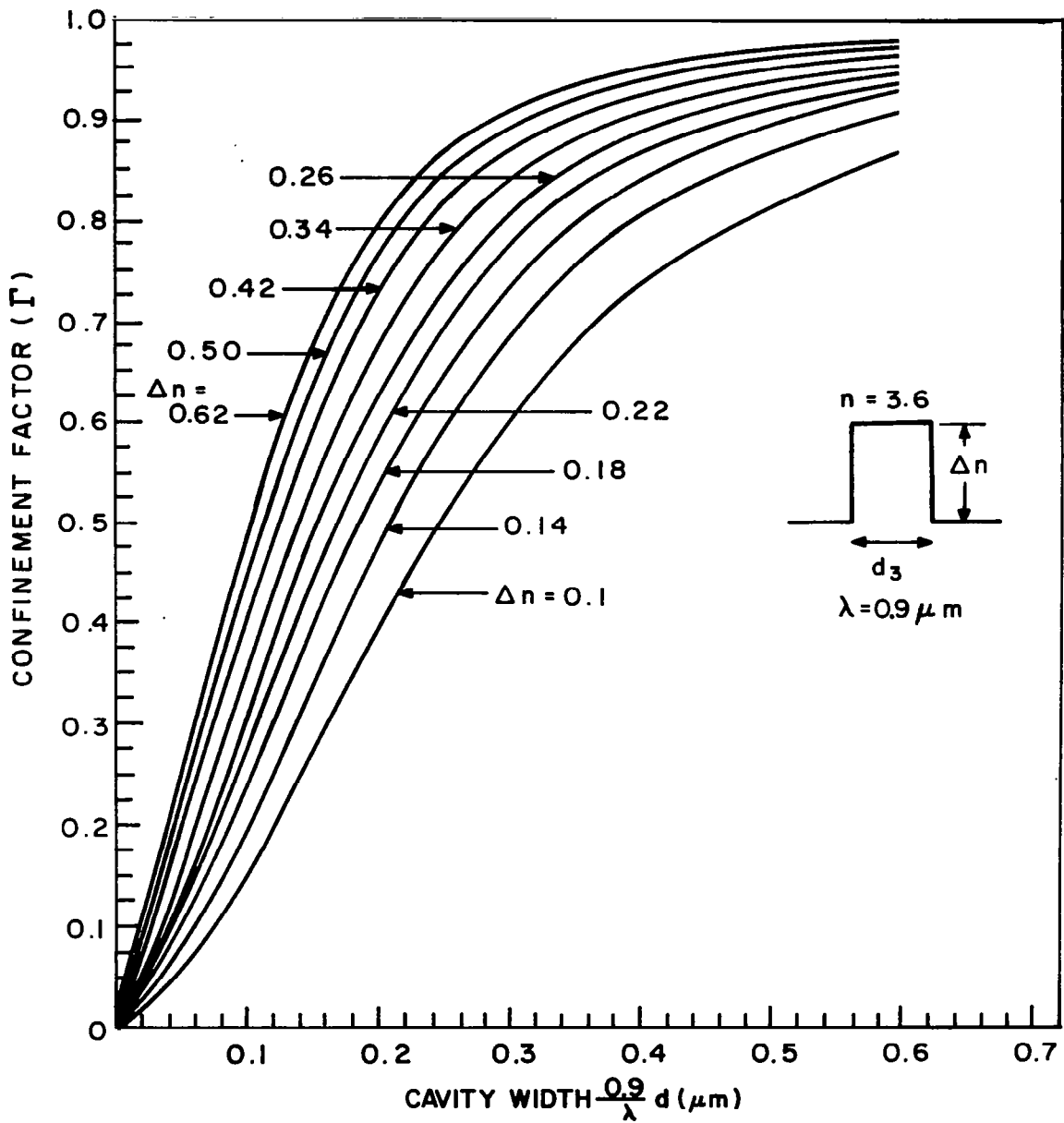


Figure 10. Theoretical radiation confinement factor Γ as a function of cavity width (J. K. Butler, unpublished).

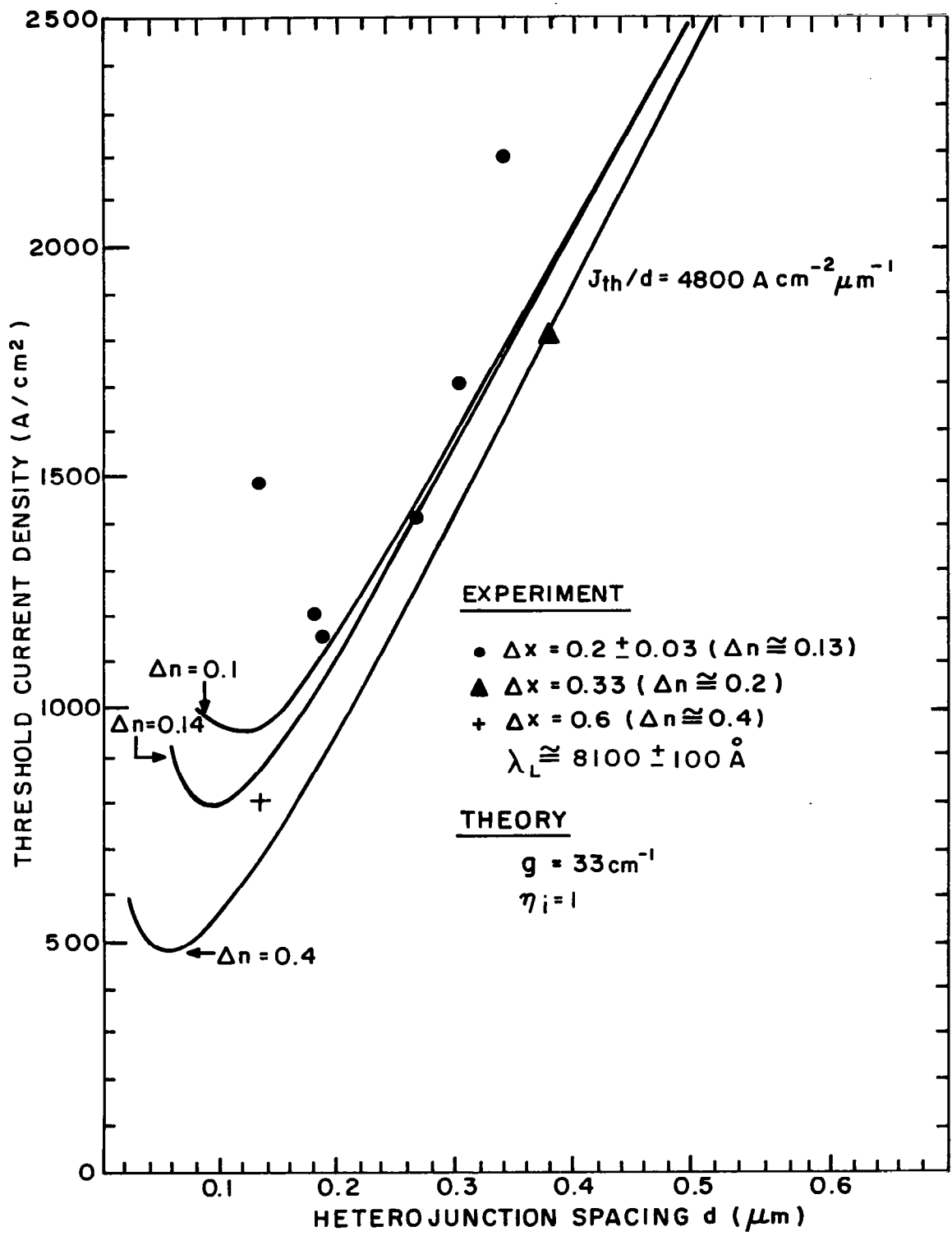


Figure 11. Theoretical dependence of J_{th} on the heterojunction spacings, d .

With other parameters constant, as a first-order approximation, the change in threshold current density with aluminum concentration in the recombination region can be predicted by simply assuming that the internal quantum efficiency is changing. This neglects the change in the J_{nom} vs g relationship with aluminum content due to changing bandshape (as reflected, for example, in the increase in the carrier effective mass, see below).

In the simplest approximation appropriate to spontaneous emission when the carrier population is nondegenerate, the ratio of the carriers in the X minima, N_X , to those in the Γ minimum, N_Γ , is determined by the ratio of the density of states and the energy difference ΔE between the Γ and X minima. The internal quantum efficiency is then defined by

$$\frac{\eta_i}{\eta_i(\text{GaAs})} = \frac{1}{1 + N_X/N_\Gamma} \quad (10)$$

where it is assumed that the carriers in the X minima make a negligible contribution to the relevant radiative processes.

When the electron population is degenerate, as appropriate under lasing conditions, then the shift of the quasi-Fermi level into the conduction band must be considered in determining the distribution of the injected carriers between the Γ and the six equivalent X minima. The carrier population is related to Fermi level by the integral of the product of density of states and of the Fermi-Dirac distribution function. Assuming parabolic bands, we obtain for the population in the Γ minimum (Ref. 10)

$$N_\Gamma = 6.55 \times 10^{21} \left(\frac{m^*}{m_{c\Gamma}} \right)^{3/2} \int_0^\infty \frac{E^{1/2} dE}{1 + \exp [(E-E_F)/kT]} \quad (11)$$

For the electron population in the X minima located ΔE above the Γ minimum,

$$N_X = 6 \times 6.55 \times 10^{21} \left(\frac{m^*}{m_{cX}} \right)^{3/2} \int_{\Delta E}^\infty \frac{(E-\Delta E)^{1/2} dE}{1 + \exp [(E-E_F)/kT]} \quad (12)$$

The following values for effective masses and separation between the direct and indirect valleys have been quoted for $\text{Al}_x\text{Ga}_{1-x}\text{As}$ (Ref. 11)

$$\begin{aligned} m_{c\Gamma}^* &= 0.0636 + 0.0552x + 0.0092x^2 \\ m_{cX}^* &= 0.39(1-x) + 0.37x \\ m_v^* (\text{AlAs}) &= 0.85 \end{aligned} \quad (13)$$

Using $\Delta E (\text{GaAs}) = 0.38$ and Eq. (1) for $E_{g\Gamma}$, we obtain

$$\Delta E(x) = 0.38 - 0.892x - 0.365x^2 \quad (14)$$

Figure 12 shows the calculated internal quantum efficiency.* If we assume that the carrier population in the Γ minimum remains at $1.5 \times 10^{18} \text{ cm}^{-3}$ irrespective of the aluminum concentration and that the radiation and carrier confinement remain constant, as does the absorption coefficient, then J_{th} increases theoretically with aluminum content

$$J_{th}(x) = \frac{J_{th}(\text{GaAs})}{\eta_i(x)} \quad (15)$$

where $\eta_i(x)$ is the internal quantum efficiency plotted in Fig. 12.

2. Horizontal Design Considerations. - As shown in our previous work (Ref. 1), one essential requirement for good diode life is to isolate regions of high current density from exposed edges. The simplest way of doing that is to use some form of stripe geometry, wherein the current is restricted to a central region of the diode, so that the lateral active diode edges are not exposed.

*We are indebted to R. Sunshine for the computer calculations.

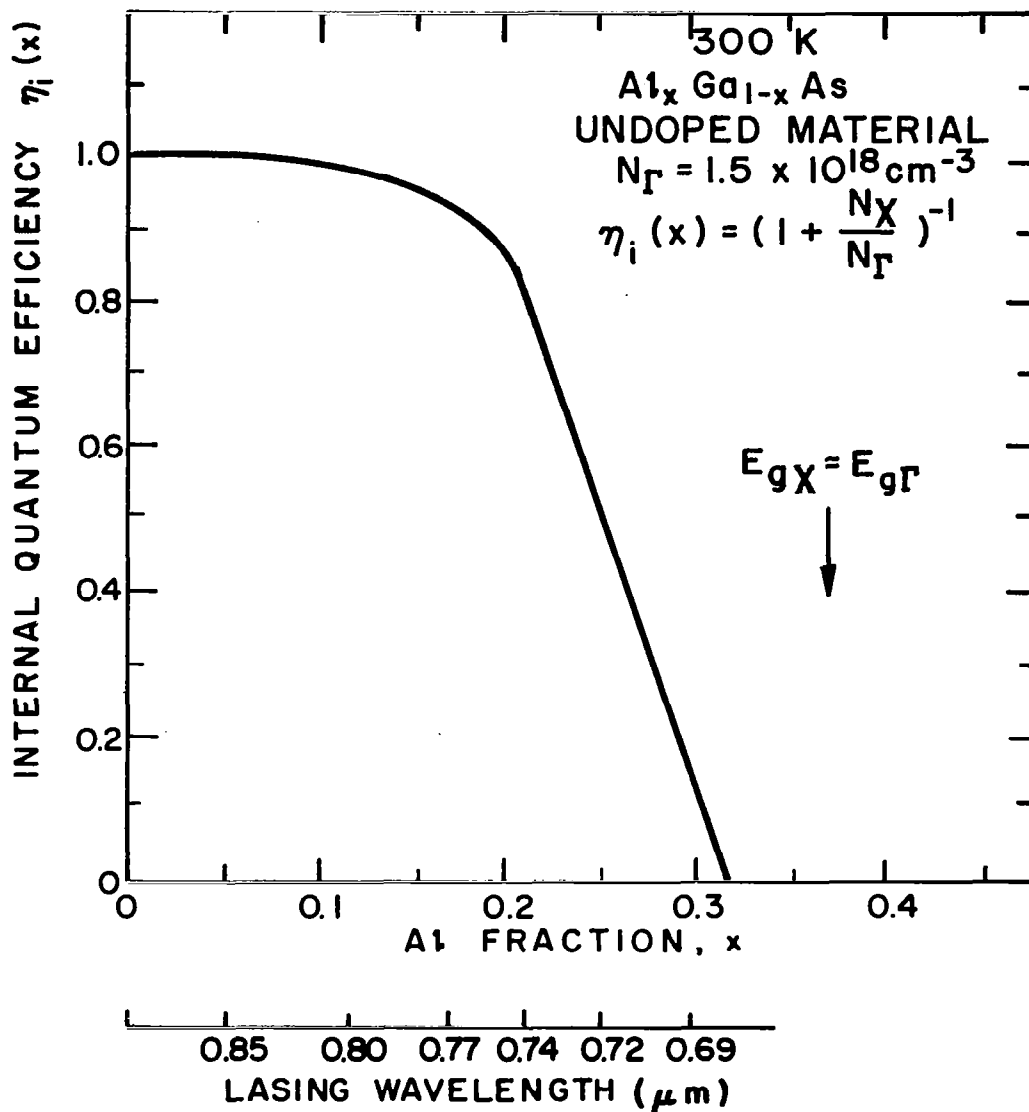


Figure 12. Calculated internal quantum efficiency as a function x , the mole fraction of Al in (AlGa)As, and the lasing wavelength.

Most of the stripe configurations used so far lead to an increase in threshold current density over that obtained for the same material in broad-area form. This arises mainly because the desire to reduce the operating current implies a corresponding reduction in the stripe width.

Associated with the width reduction, however, there arise a number of loss mechanisms which serve to increase the threshold current *density*. Thus, various stripe configurations have to be carefully evaluated as regards their effect on operating current density, because the current density controls the degradation mechanism limiting the diode life.

One of the most important factors limiting the performance of planar stripe lasers is the current spreading beyond the edge of the stripe. (There are other factors which influence the stripe threshold, but we shall neglect them in this analysis.) As shown in Fig. 13, this lateral

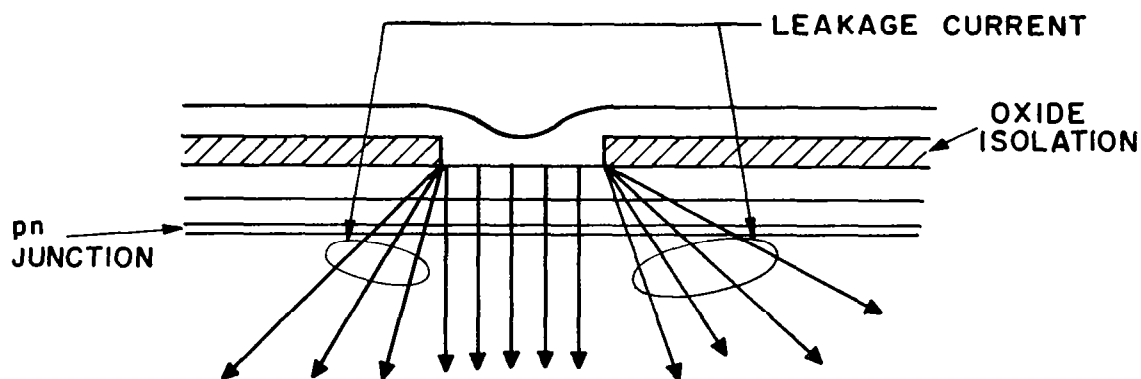


Figure 13. Leakage current at edges of stripe laser.

current flow widens the emission beyond the area under the stripe, and increases the threshold current density beyond that obtained for the same material when it is fabricated into a wide unit. Following several published analyses [e.g., (Ref. 12)] the lateral current flow can be obtained from the following differential equation:

$$\frac{\partial^2 \phi}{\partial y^2} = e \phi \quad (16)$$

where y is a normalized distance and ϕ is a normalized potential. The solution of this equation, with the appropriate boundary conditions,

can be shown to yield the following expression for the extra current flowing beyond the stripe edges (for a diode of unit length):

$$I = 2 \sqrt{\frac{2J_{\infty}}{R_s \alpha}} \quad (17)$$

where J_{∞} is the broad-area threshold current density, R_s is the sheet resistivity of the layers between the contact and the p-n junction, and $\alpha = q/nkT$ with $n \approx 2$. If W is the stripe width, then the total current through a stripe diode of unit length, at threshold, will be given by

$$I_{\text{stripe}} = J_{\infty} W + 2 \sqrt{\frac{2J_{\infty}}{R_s \alpha}} \quad (18)$$

and the ratio of J_{stripe} to J_{∞} , or the increase in threshold current density, by

$$\frac{J_{\text{stripe}}}{J_{\infty}} = 1 + \frac{2}{W} \sqrt{\frac{2}{R_s \alpha J_{\infty}}} \quad (19)$$

In estimating the importance of this effect, the key parameter is R_s , the average sheet resistivity of the top layers. While estimates of this quantity can be made from the known melt compositions, and the measured layer thicknesses, we outline a measurement procedure which yields this value directly. As shown in Fig. 14, we take a strip of material, containing a series of stripes (which would normally be processed into diodes by separating between the stripes), and remove the metallization bridging one stripe with the next. The separation of the strips and the width of the strips are both large compared with the thickness of the layers, so that we can safely neglect the complications of nonuniform current flow near the electrodes. If we apply a

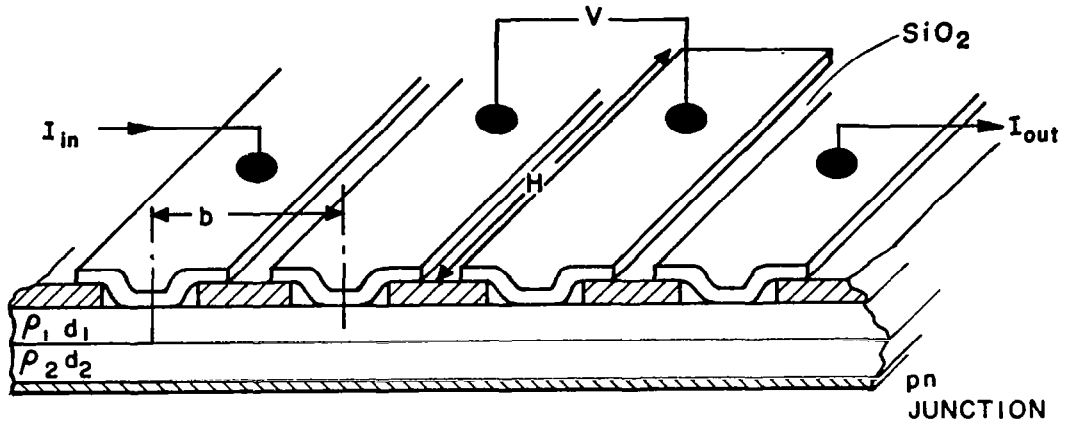


Figure 14. Sheet resistivity measurement.

current I between two outer electrodes and measure a voltage V between two inner electrodes, then it is easily shown that

$$R = \frac{V}{I} = \frac{b}{H} \left(\frac{1}{\frac{d_1}{\rho_1} + \frac{d_2}{\rho_2}} \right) \quad (20)$$

where H is the length of the electrodes, b is their separation, and d_i, ρ_i are thickness and resistivity of the i^{th} layer.

In the case of a single layer with resistivity ρ and thickness d , we have

$$R = \frac{b}{H} \left(\frac{\rho}{d} \right) = \frac{b}{H} R_s \quad (21)$$

which defines the sheet resistivity R_s .

In the present case, using Eq. (20), the combined sheet resistivity R_s is given by

$$R_s = \frac{\rho_1 \rho_2}{\rho_2 d_1 + \rho_1 d_2} = R \frac{H}{b} \quad (22)$$

It is now convenient to use the measured values of R_s in Eq. (19) to compare calculated and experimental thresholds. Figure 15 shows experimental data on a number of units together with a plot of Eq. (19)

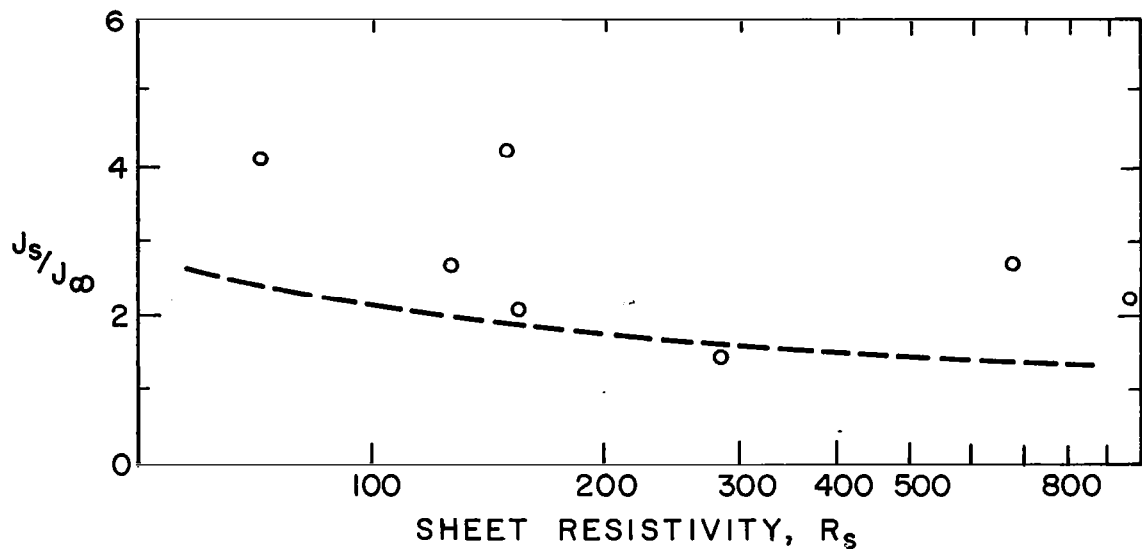


Figure 15. J_s/J_∞ for a number of diodes made from different wafers. A plot of Eq. (19) with $W = 13 \mu\text{m}$ and $J_\infty = 2000 \text{ A/cm}^2$ is also shown.

with $J_\infty = 2000 \text{ A/cm}^2$. Some of the R_s values were measured, and some calculated from Eq. (22). There is a great deal of scatter, most likely because of uncertainties in the data due to sample-to-sample variations in the threshold currents. Equation (19) is not too useful as it stands, but it indicates the trend of the experimental values. It can be noted that a J_s/J_∞ ratio as low as 1.45 was obtained in one case, indicating an extremely low leakage current.

To reduce the resistance of the p-contact, zinc diffusions have been performed after the oxide isolation has been applied. The main problem in these zinc diffusions seems to be the need to prevent the zinc from penetrating too far into the p-wall region.

We have begun the investigation of another scheme for reducing the threshold current, called the "inverted stripe" configuration, in which the current constriction is grown into the device rather than being applied externally. Considerable problems were encountered due to crystallographic effects, one of which is the tendency of the etch to

undercut the sides of the depression. This work is presently at a very early stage.

D. Experimental Laser Results

To obtain the lowest possible J_{th} in the visible portion of the spectrum, the lasers were fabricated with $d \approx 0.1 \mu\text{m}$ and the highest aluminum fraction ($y \approx 0.6$) which could be conveniently accommodated in the bounding regions. Thus, the aluminum difference $y - x$ between the recombination region and the outer two regions of the symmetrical $\text{Al}_y\text{Ga}_{1-y}\text{As}/\text{Al}_x\text{Ga}_{1-x}\text{As}$ DH lasers decreased with x . The p-type $\text{Al}_{0.6}\text{Ga}_{0.4}\text{As}$ region was highly doped with Zn ($\sim 10^{19} \text{cm}^{-3}$), while the n-type $\text{Al}_{0.6}\text{Ga}_{0.4}\text{As}$ region was Te-doped ($1-2 \times 10^{18} \text{cm}^{-3}$). The recombination region was not deliberately doped. The distance between the active region and the heat sink is $\sim 2 \mu\text{m}$ and is divided between a $1\text{-}\mu\text{m}$ -thick $\text{Al}_{0.6}\text{Ga}_{0.4}\text{As}:\text{Zn}$ layer and a $\text{GaAs}:\text{Zn}$ ($\sim 10^{19} \text{cm}^{-3}$) cap region to facilitate ohmic contact as shown in Fig. 16.

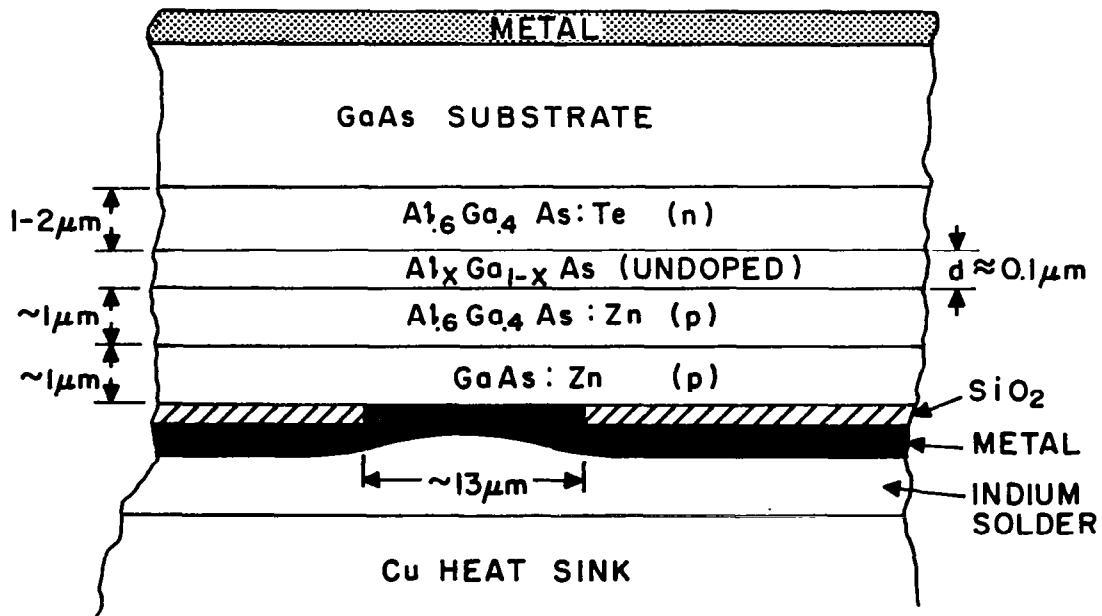


Figure 16. Cross section (not to scale) of low-threshold laser diodes with $x \lesssim 0.2$.

The use of zinc (with its high vapor pressure) entails potential problems of cross-contamination of the solutions within the multiple-bin boat used for the liquid-phase epitaxial growth. The fabrication of the shortest-wavelength visible lasers was made possible by the use of an unusually high growth rate (2.5 $\mu\text{m}/\text{min}$), which minimizes the cross-contamination problem. Thus, the devices were grown under conditions which can be considered to be nonequilibrium. A starting temperature of approximately 900°C was selected because of the perfect lattice match between AlAs and GaAs at that temperature (Ref. 13).

The lasers were measured under pulsed operation in the form of conventional broad-area structures (100 μm x 500 μm). For cw operation, stripe-contact structures using SiO_2 isolation were made with 13- μm -wide stripes. These were mounted p-side down on a copper header and measured at a heat sink temperature of 20°C. In some cases selective zinc diffusion was performed to improve the ohmic contact as described in Section III.A.

Table I lists the lowest threshold current density values achieved in pulsed operation of the broad-area devices using the fast-cool growth

TABLE I. LASER DATA (300 K)

Wavelength λ_L (Å)	J_{th} (A/cm ²)	η_{ext} (%)
8800	800	35
7760	800	35
7690	900	24
7530	1140	14
7400	1300	24
7240	2230	14
6900	30,000	3

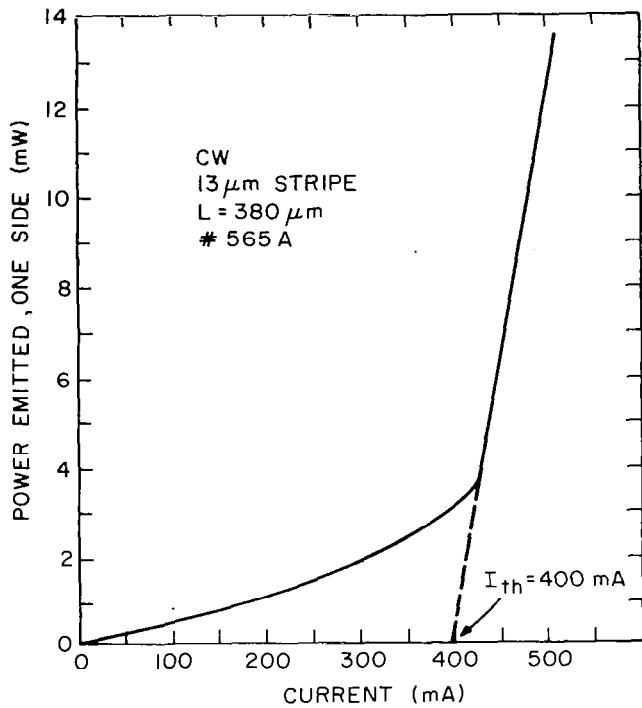
*Broad-area diodes, 100 μm x 500 μm ; pulsed operation: 100-ns pulse length, 1-kHz rate; two-sided emission.

process. As shown in the table for $\lambda_L = 7240 - 8000 \text{ \AA}$, these values are at least half those previously reported at similar wavelengths (Refs. 14-17) and are in the range where cw operation is feasible (thermal device properties permitting). In our experiments, cw room-temperature operation was limited to lasers with $\lambda_L \geq 7400 \text{ \AA}$ because of the relatively high thermal resistance of the shorter wavelength devices. This represents the shortest cw lasing wavelength reported to date for a laser diode at room temperature.

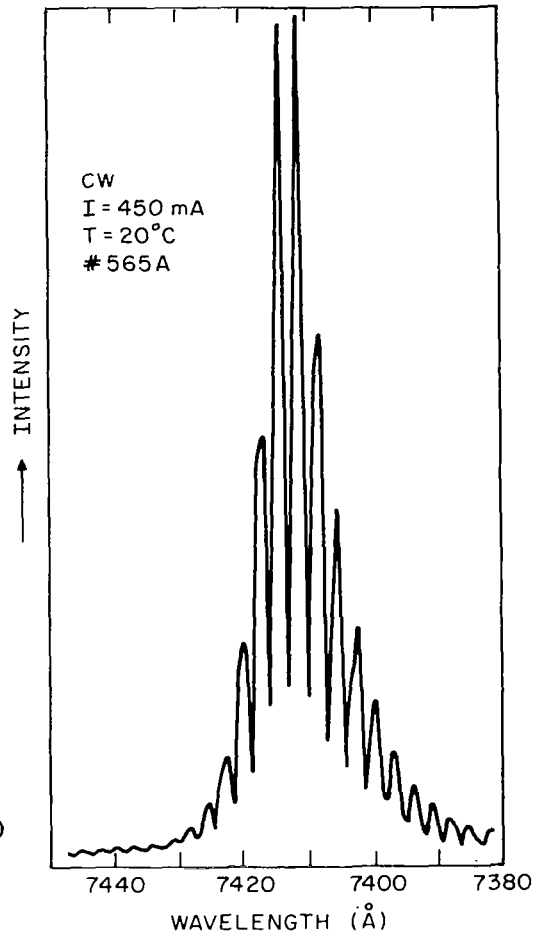
The performance characteristics of a typical cw laser emitting at about 7400 \AA is shown in Fig. 17. Figure 17(a) shows the curve of power emitted vs direct current (one-sided emission). The curve is limited to 12 mW, although power values as high as 25 mW have been obtained. These, however, are in the range where facet damage may occur (Appendix A). The threshold current of this device was 400 mA, a value reflecting the fact that lateral current spreading is significant due to the high conductivity of the p-type layers of this wafer between the active region and the surface. Near-field observations show that the effective laser emitting region is 40 \mu m wide; (the cw threshold current density is $\sim 2600 \text{ A/cm}^2$ while the broad-area $J_{th} = 1300 \text{ A/cm}^2$). In Fig. 17(b) we show the spectral emission at 450 mA where the power emitted is 6 mW. The spectral lines are limited to a few longitudinal modes. The far-field pattern of this laser (with $d = 0.08 \text{ \mu m}$) is shown in Fig. 17(c) in the direction perpendicular to the junction plane. The beam width of 52 deg is consistent with the value calculated using the expression (Ref. 18) valid for a very small value of d

$$\theta_{\perp} \cong 20 \frac{d (y-x)}{\lambda_L} \quad (\text{radians}) \quad (23)$$

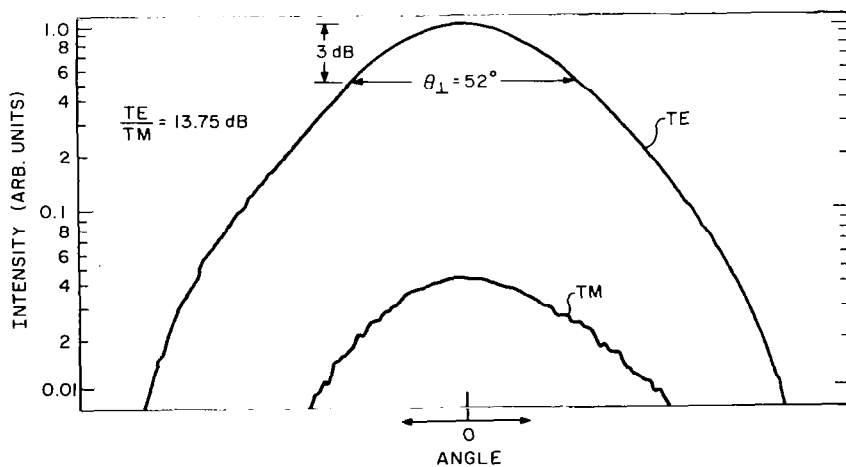
the recombination region and the bounding walls. With $d = 0.08 \text{ \mu m}$, $\lambda_L = 0.74 \text{ \mu m}$, and $(y-x) = 0.4$ ($\Delta n = 0.26$), we obtain $\theta_{\perp} = 49 \text{ deg}$.



(a)



(b)



(c)

Figure 17. Performance characteristics of laser diode operating cw at room temperature. (a) Power output, one side, as a function of current. (b) Spectral emission at 450 mA (6 mW of power emitted). (c) Far-field pattern in the direction perpendicular to the junction plane.

To compare the threshold current density of the broad-area 7400-Å unit with theory, we have to determine the confinement factor. Using the measured beam pattern, we obtain (Ref. 18)

$$\Gamma = \frac{d\theta_{\perp}}{0.205\lambda} = 0.47 \quad (24)$$

With an assumed absorption coefficient $\alpha = 10 \text{ cm}^{-1}$, $L = 500 \text{ }\mu\text{m}$, we estimate $g = 33 \text{ cm}^{-1}$. Hence, from Eq. (9), using Fig. 12 to estimate a relative $\eta_i = 0.8$ and assuming a GaAs internal quantum efficiency of 0.7, the predicted threshold current density would be 800 A/cm^2 . The measured value of 1300 A/cm^2 is not unreasonable, considering the approximations. The difference, however, leaves room for other factors to degrade J_{th} with increasing x .

To explore the comparative increase in J_{th} with aluminum content for the other devices tested, we compare in Fig. 18 the lowest observed J_{th} values for each x value with the internal quantum efficiency increase, taking $J_{\text{th}} = 800 \text{ A/cm}^2$ (obtained for 8000-Å lasers made with the fast-cool zinc-doping process) as a point of reference. Figure 18 shows that the experimental J_{th} values increase faster than expected on the basis of the calculated internal quantum efficiency increase. Several factors may contribute to this increase: (1) Lack of constant radiation confinement because the barrier height is decreasing as the aluminum content is increasing in the recombination region. For example, at $\lambda_L = 8000 \text{ Å}$, $y-x = 0.5$, while at $\lambda_L = 7000 \text{ Å}$, $y-x = 0.32$. (2) A decreasing material quality, or strain effects.

The experiments conducted using the hydrostatic pressure apparatus* provide some evidence for anomalous changes in the threshold dependence possibly related to material changes. It is not known, however, whether these changes are related to the material growth process. For example, stoichiometric factors are believed affected by the growth method.

*Experiments conducted under subcontract at Yeshiva University by Y. Juravel and P. M. Raccah.

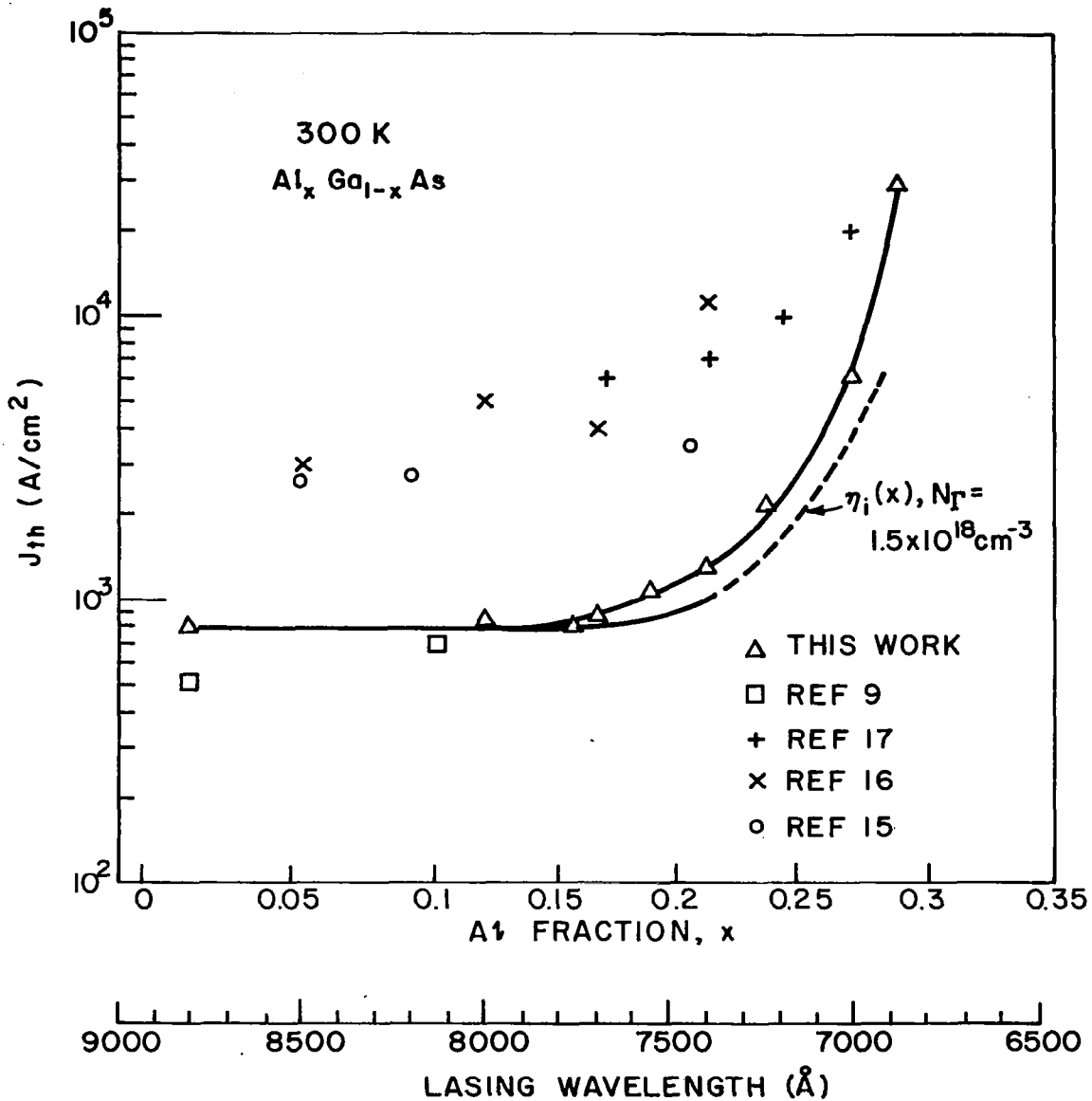


Figure 18. Room-temperature threshold current densities of DH (AlGa)As laser diodes vs emission wavelength. This work is compared with the lowest J_{th} values reported in the literature.

Note that the diodes studied so far by hydrostatic measurements were early diodes not grown by the process which is now giving us the lowest threshold lasers.

Figure 19 shows the dependence of the threshold change with pressure as a function of x . The effect of the hydrostatic pressure is to *raise* the Γ conduction band minimum by about 10.7 meV/kb while the X minima are decreased by ~ 1.1 meV/kb (Ref. 19); the net effect is that the separation ΔE between the Γ and X minima is decreased by about 11.8 meV/kb. Considering the simplest model of the change in internal quantum efficiency resulting from the reduction in the ΔE reduction, the change in the normalized J_{th} with pressure should follow an expression of the form

$$\frac{1}{J_{th}(0)} \frac{\partial J_{th}}{\partial P} = \frac{1}{J_{th}(0)} \frac{\partial}{\partial P} \left(\frac{1}{1 + \frac{N_X}{N_\Gamma}} \right) \quad (25)$$

where $J_{th}(0)$ is the value at atmospheric pressure. Figure 19 shows the calculated dependence of Eq. (25) for lasers having varying aluminum concentrations in the recombination, assuming different values of the carrier population in the recombination region. Note that the J_{th} is more pressure-sensitive than expected on the basis of this model. It is possible that defects are becoming active in the recombination region with pressure and thus depress the internal quantum efficiency. However, to explain the observed effect, it is necessary to postulate that the density of such defects increases with the aluminum concentration in the recombination region. Anomalous pressure-dependent effects (under uniaxial stress) have also been reported by Kobayashi and Sugiyama (Ref. 20) in $\text{Al}_x\text{Ga}_{1-x}\text{As}$, which may be explained by defects.

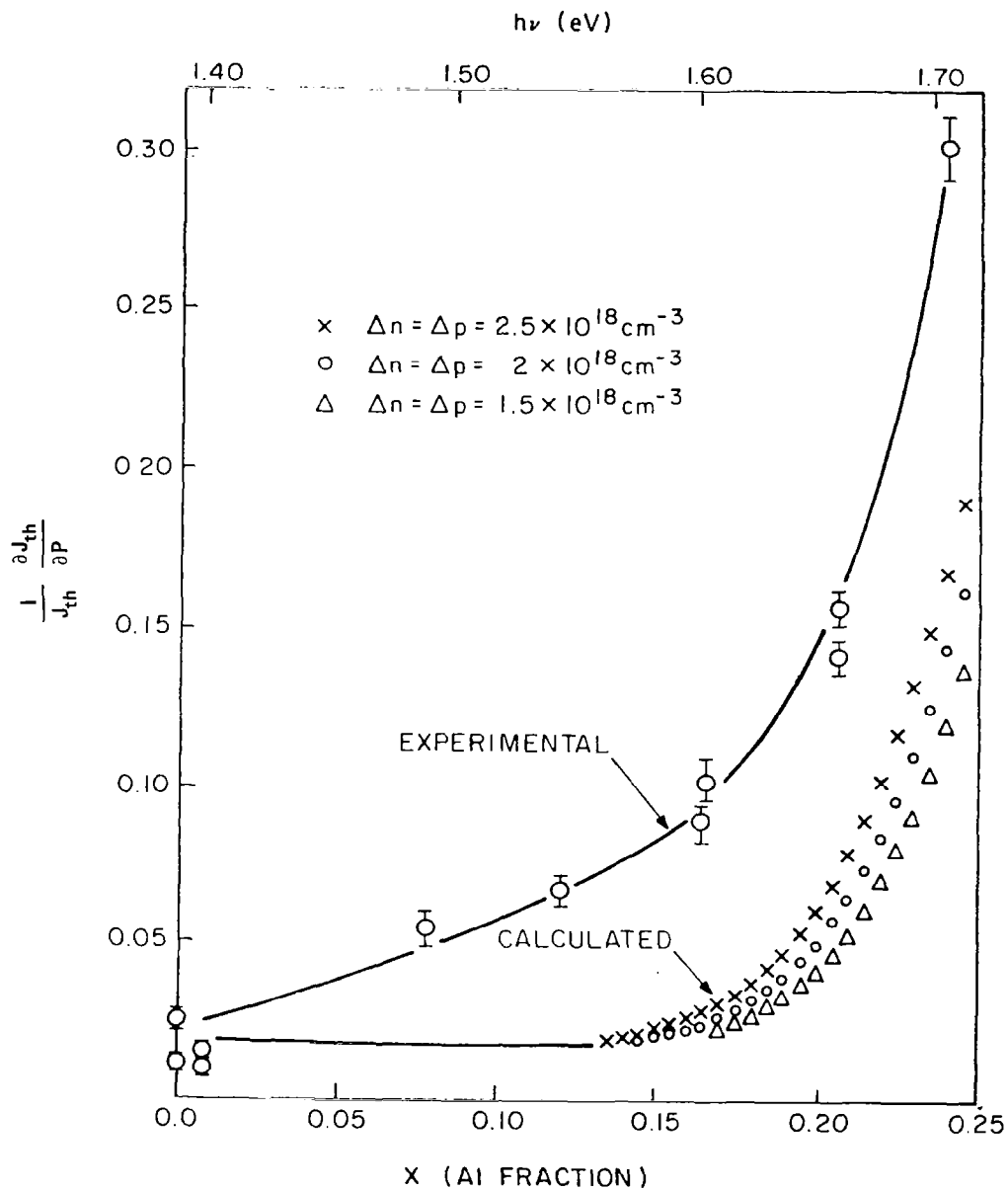


Figure 19. Comparison of experimental data and theory on the hydrostatic pressure dependence of the threshold current density of (AlGa)As lasers (work of Y. Juravel and P. M. Raccah, Yeshiva University).

III. VAPOR-PHASE GROWTH OF $\text{GaAs}_{1-x}\text{P}_x/\text{In}_y\text{Ga}_{1-y}\text{P}$ HETEROJUNCTION LASER STRUCTURES

Recently, lattice-matched heterojunction laser structures of $\text{GaAs}/\text{In}_y\text{Ga}_{1-y}\text{P}$ (Ref. 21) and $\text{In}_x\text{Ga}_{1-x}\text{As}/\text{In}_y\text{Ga}_{1-y}\text{P}$ (Ref. 22) have been prepared by a vapor-phase growth technique. These structures utilize the concept of lattice matching that has been extensively applied throughout the $\text{Al}_x\text{Ga}_{1-x}\text{As}$ alloy system to reduce the introduction of misfit dislocations at the epitaxial interfaces, and have yielded room-temperature lasers with threshold current densities as low as 8000 A/cm^2 (Ref. 23). Because of the success of the recent vapor-grown GaAs and $\text{InGa}_{1-x}\text{As}$ structures, we have attempted to prepare similar structures of $\text{GaAs}_{1-x}\text{P}_x/\text{In}_y\text{Ga}_{1-y}\text{P}$ for visible-light-emitting lasers. The principles used in the preparation of these structures and the results of preliminary experiments performed under this contract are described below.

A. Lattice Matching $\text{GaAs}_{1-x}\text{P}_x$ with $\text{In}_y\text{Ga}_{1-y}\text{P}$

The lattice constant of $\text{In}_y\text{Ga}_{1-y}\text{P}$ alloys span a range from 5.451 \AA (for GaP) to 5.869 \AA (for InP), and therefore can be used to lattice match any desired alloy of $\text{GaAs}_{1-x}\text{P}_x$, whose lattice constant ranges between 5.451 \AA (for GaP) and 5.653 \AA (for GaAs). For a particular alloy of $\text{GaAs}_{1-x}\text{P}_x$ the unique lattice-matching alloy of $\text{In}_y\text{Ga}_{1-y}\text{P}$ can be determined from the expression:

$$y = 0.483 (1-x) \tag{26}$$

For emission near 7000 \AA , the $\text{GaAs}_{1-x}\text{P}_x$ alloy composition should have $x = 0.3$; from Eq. (26), the appropriate $\text{In}_y\text{Ga}_{1-y}\text{P}$ composition for lattice matching $\text{GaAs}_{.7}\text{P}_{.3}$ should therefore have $y = 0.34$.

The energy bandgap for alloys of $\text{In}_y\text{Ga}_{1-y}\text{P}$ and $\text{GaAs}_{1-x}\text{P}_x$ at their lattice-matching compositions is illustrated in Fig. 20. Immediately apparent here is the energy difference of about 0.5 eV over the wavelength range of interest. This difference is very large for heterojunction lasers

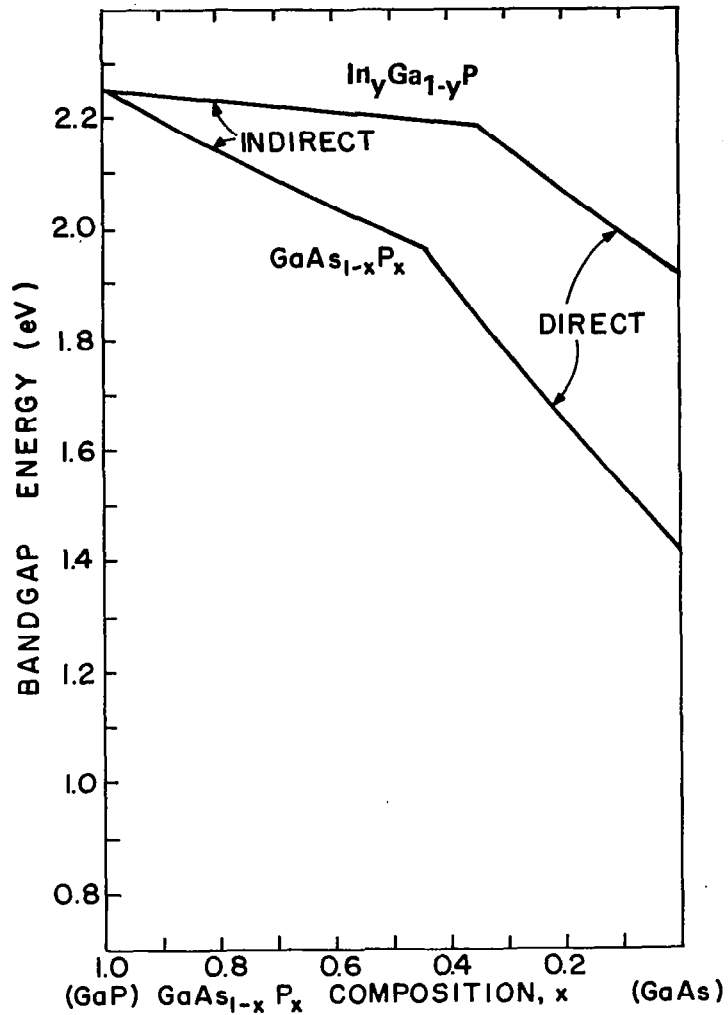


Figure 20. Room-temperature energy-bandgap values of $\text{In}_{1-y}\text{Ga}_y\text{P}$ and $\text{GaAs}_{1-x}\text{P}_x$, alloys for lattice-matched structures of $\text{In}_{1-y}\text{Ga}_y\text{P}/\text{GaAs}_{1-x}\text{P}_x$.

and should readily confine the injected carrier in the active $\text{GaAs}_{1-x}\text{P}_x$ laser cavity. The refractive index of $\text{In}_y\text{Ga}_{1-y}\text{P}$ alloys has not been studied extensively; however, a few preliminary measurements[†] indicate a

[†]P. Zanzucchi, private communication.

refractive index value of about 3.3, which is sufficiently lower than that of $\text{GaAs}_{1-x}\text{P}_x$ to provide efficient optical confinement. Hence, alloys of $\text{GaAs}_{1-x}\text{P}_x$ and $\text{InGa}_{1-y}\text{P}$ seem like a reasonable choice for room-temperature heterojunction lasers. The principles used for the preparation of these materials are described below.

B. Vapor-Phase Growth

The apparatus used to prepare alloys of $\text{GaAs}_{1-x}\text{P}_x$ and $\text{InGa}_{1-y}\text{P}$ is shown schematically in Fig. 21. For the growth of $\text{InGa}_{1-y}\text{P}$, the use of separate quartz tubes to contain the In and Ga sources allows independent

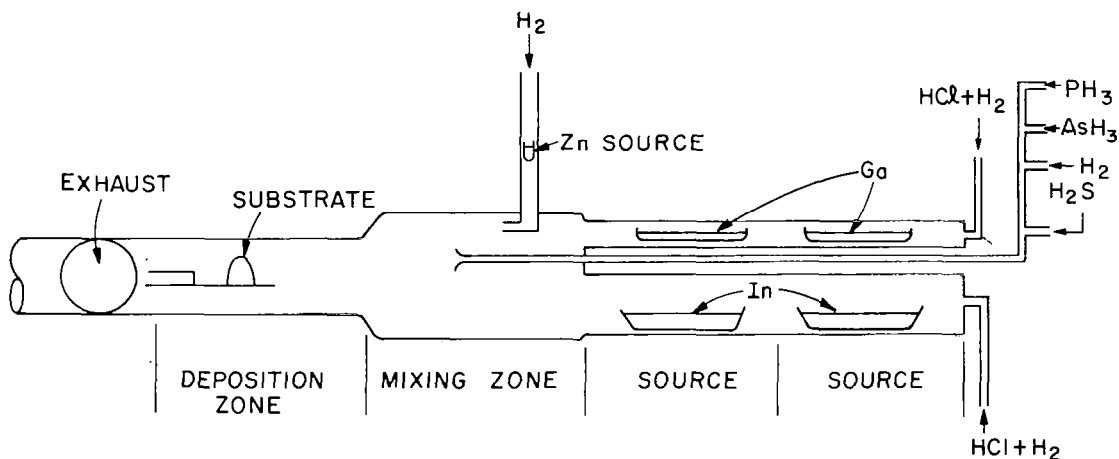
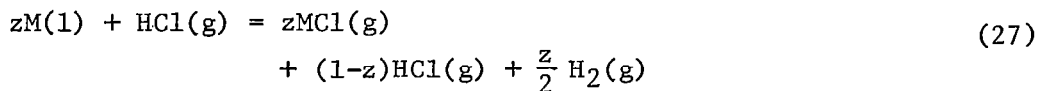
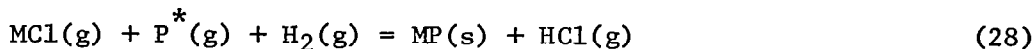


Figure 21. Schematic diagram of the vapor-phase growth system used for the epitaxial deposition of single-crystalline layers of $\text{InGa}_{1-y}\text{P}$ and $\text{GaAs}_{1-x}\text{P}_x$.

control of the HCl concentrations over each of the metal sources. Mass spectrometric analysis of the gases in the growth tube has shown that HCl reacts with Ga and In metals to form monochlorides of these metals according to the reaction



Here M is In or Ga and z is the mole fraction of HCl consumed in the reaction. The metal monochlorides are carried in hydrogen into the mixing zone where they mix, but do not react, with gaseous phosphine, the source of phosphorus. The reduced temperature in the deposition zone, where the substrate is positioned, allows the reaction between gases to give $\text{In}_y\text{Ga}_{1-y}\text{P}$ as an epitaxial film and HCl as the gaseous by-product according to the reaction



Here, P^* represents PH_3 and the products of the decomposition of PH_3 , namely P_2 and P_4 .

For the growth of $\text{GaAs}_{1-x}\text{P}_x$, the chemical reactions are similar, except for the addition of AsH_3 in the mixing zone with its major decomposition species, As_2 and As_4 . For the growth of $\text{GaAs}_{1-x}\text{P}_x$, no HCl is passed over the In source, eliminating InCl as a transport agent for the group III metals.

Finally, a p-n junction is formed during vapor deposition by sequentially introducing H_2S (as the source of the donor, sulfur) and zinc (carried in a hydrogen stream) into the deposition region of the reactor. This *in situ* p-n junction formation technique eliminates the need of a post-growth high-temperature diffusion step and significantly simplifies the technology for preparing heterojunction lasers of different materials.

C. Structure

The structure used for our experiments is shown in Fig. 22. Here, the substrate consists of an n-type commercial $\text{GaAs}_{.7}\text{P}_{.3}$ epitaxial wafer.* This wafer was oriented in the <100> crystallographic direction and was doped with Te to a donor concentration of $1-2 \times 10^{17} \text{ cm}^{-3}$. The portion

*Monsanto Co., St. Louis, Mo.

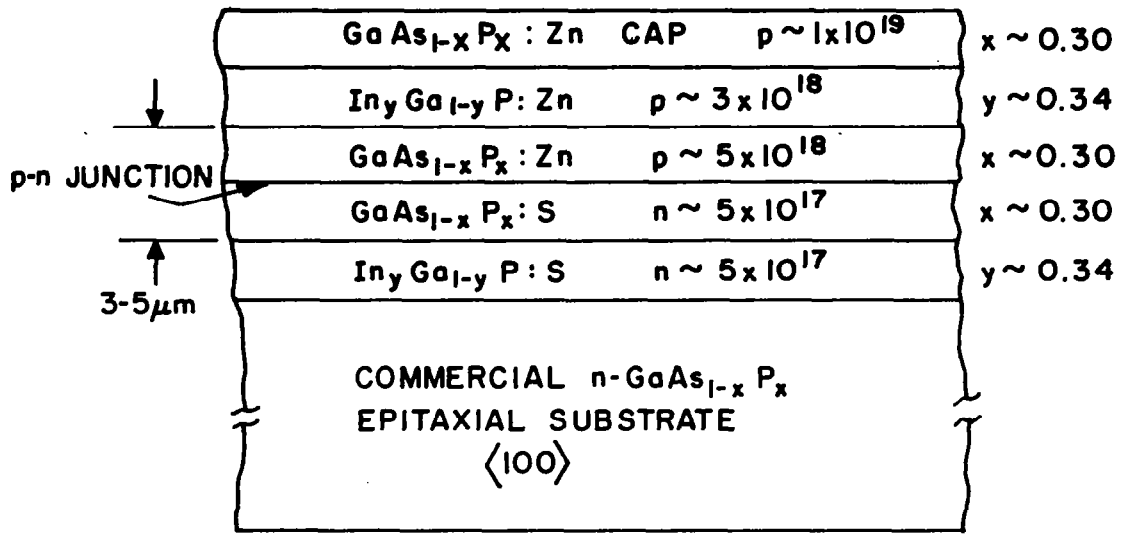


Figure 22. Schematic presentation of vapor-grown $\text{GaAs}_{1-x}\text{P}_y/\text{In}_y\text{Ga}_{1-y}\text{P}$ heterojunction structure prepared for visible-light-emitting laser diodes.

of the structure grown in our laboratory consisted of the two $\text{In}_y\text{Ga}_{1-y}\text{P}$ ($y \sim 0.34$) confining layers, each 2 to 3 μm thick, and a $\text{GaAs}_{1-x}\text{P}_x$ ($x \sim 0.3$) laser cavity, 3 to 4 μm thick, containing a p-n junction approximately in its center. A zinc-doped $\text{GaAs}_{1-x}\text{P}_x$ "cap" was employed as the final layer to facilitate making ohmic contact to the higher-bandgap p-type $\text{In}_y\text{Ga}_{1-y}\text{P}$ uppermost confining layer. The n-type layers of $\text{GaAs}_{1-x}\text{P}_x$ and $\text{In}_y\text{Ga}_{1-y}\text{P}$ were doped with sulfur (from H_2S) to a carrier concentration of about $5 \times 10^{17} \text{ cm}^{-3}$, while the p-type $\text{GaAs}_{1-x}\text{P}_x$ and $\text{In}_y\text{Ga}_{1-y}\text{P}$ layers were zinc-doped to a carrier concentration between 3×10^{18} and $1 \times 10^{19} \text{ cm}^{-3}$.

Although it would have been most desirable to prepare the epitaxial layers of $\text{In}_y\text{Ga}_{1-y}\text{P}$ and $\text{GaAs}_{1-x}\text{P}_x$ sequentially in a single vapor-phase reactor, this was not possible for the wafers prepared to date. Previously, all of the $\text{GaAs}_{1-x}\text{P}_x$ electroluminescent structures had been prepared in one particular reactor, whereas most of the lattice-matched $\text{In}_y\text{Ga}_{1-y}\text{P}$ heterojunction lasers had been prepared in another reactor. We therefore attempted to prepare the structure shown in Fig. 22 in several steps.

We first deposited the $\text{In}_y\text{Ga}_{1-y}\text{P}$ layer on the commercial $\text{GaAs}_{1-x}\text{P}_x$ substrate and then removed the wafer from the first reactor and immediately inserted it into a second reactor to prepare the $\text{GaAs}_{1-x}\text{P}_x$ p-n junction layers. Next, the wafer was removed from the second reactor and reinserted into the first reactor for the growth of the uppermost $\text{In}_y\text{Ga}_{1-y}\text{P}$ confining layer. In this way, we were able to take advantage of the proper flow conditions, temperatures, gradients, etc., that had been previously established for optimum growth of $\text{GaAs}_{1-x}\text{P}_x$ and $\text{In}_y\text{Ga}_{1-y}\text{P}$ epitaxial layers. Admittedly, this advantage was at the expense of exposing the wafer to the ambient for a brief time (~1 min) at each of the transitions between these two materials. Obviously, in future experiments, the growth should be optimized for both $\text{In}_y\text{Ga}_{1-y}\text{P}$ and $\text{GaAs}_{1-x}\text{P}_x$ in a single reactor.

D. Laser Properties

In each of three such heteroepitaxial structures, laser operation was obtained at 77 K, with threshold current densities of about 3000 to 5000 A/cm^2 and emission wavelengths of 6520 to 6640 Å. These values, which are not low for the $\text{GaAs}_{1-x}\text{P}_x$ alloy system, reflect the fact that the p-n junction formation techniques as well as the donor and acceptor concentrations had not been optimized. Nonetheless, the temperature dependence of one of the heterojunction lasers was found to vary by only a factor of 10 between 77 and 273 K, indicative of effective optical confinement in these structures. For example, our early $\text{GaAs}/\text{In}_y\text{Ga}_{1-y}\text{P}$ and $\text{In}_x\text{Ga}_{1-x}\text{As}/\text{In}_y\text{Ga}_{1-y}\text{P}$ laser structures had similar temperature dependences, although their 77 K threshold values were about an order of magnitude lower than those of the $\text{GaAs}_{1-x}\text{P}_x$ lasers. Interestingly, two homojunction laser structures of $\text{GaAs}_{1-x}\text{P}_x$ also were prepared and evaluated. These were found to have threshold current densities slightly higher than the heterojunction structures, confirming that the junctions themselves are not of state-of-the-art quality in these initial structures. A representative J_{th} dependence on T of these heterojunction lasers is shown in Fig. 23. The highest

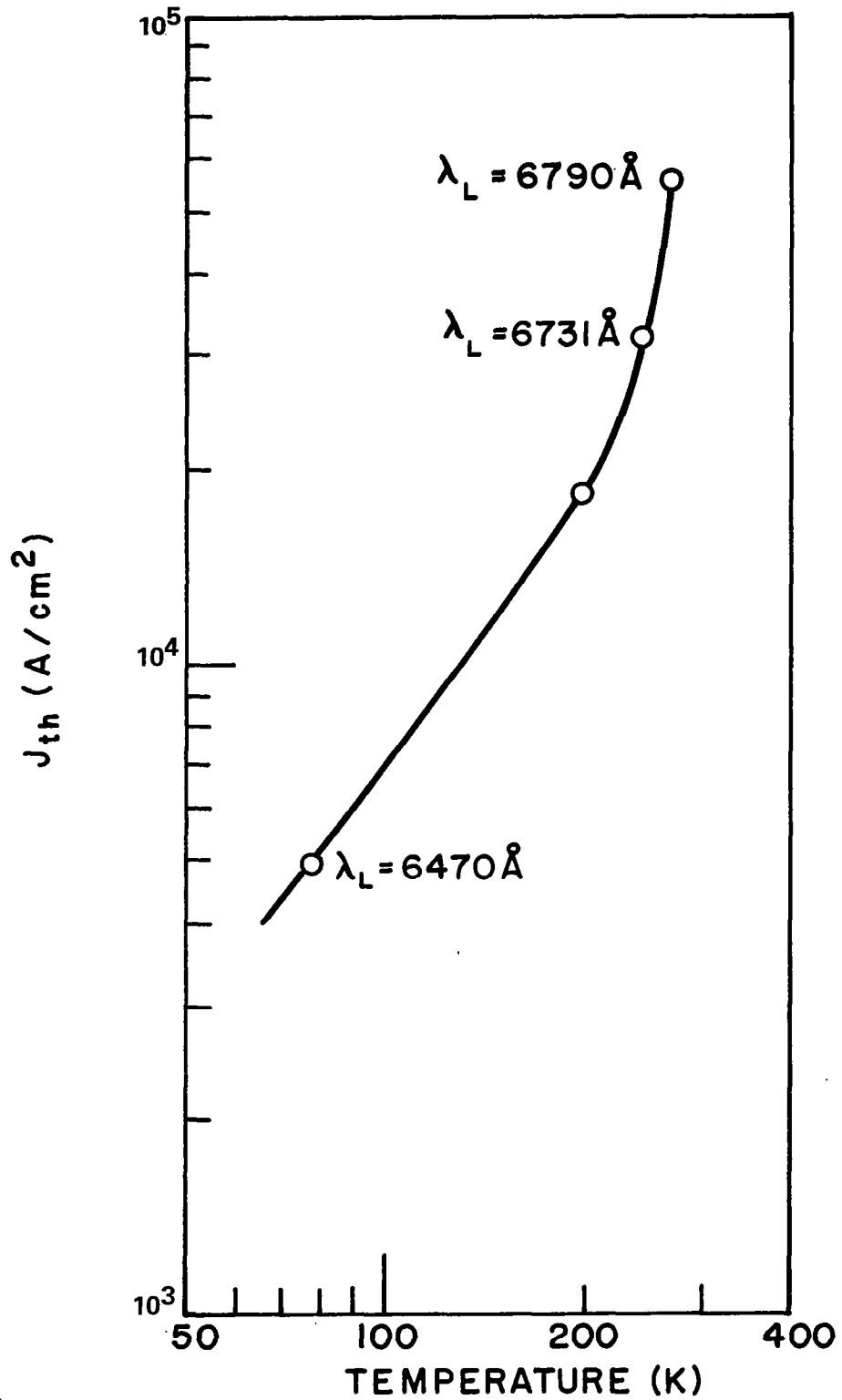


Figure 23. Threshold current dependence of heterojunction laser (InGaP/GaAsP).

temperature at which lasing was observed was 273 K, with $\lambda_L = 6790 \text{ \AA}$. Figure 24 shows the shifting emission lines with current as lasing is approached at 77 K. This shifting, which is quite large, most likely results from bandfilling, although radiative tunneling may be a factor at the low current levels.

The fact that the junction quality is relatively poor in these devices is reflected in the light-output vs current curve. Figure 25 compares the light output vs current at room temperature (in the spontaneous emission mode) of one of these devices with a $\text{Al}_{.5}\text{Ga}_{.5}\text{As}/\text{GaAs}$ heterojunction. Note that the output of the latter device is linear with current (until lasing threshold sets in). For the $\text{GaAsP}/\text{InGaP}$ diode, on the other hand, the slope exceeds one, indicating that a substantial fraction of the current is nonradiative, an effect associated with the defects in the active region and/or the interface. It is expected that improved diode properties, obtained by better growth, will improve these properties as well as the lasing characteristics. A direct example of the effect of the lattice parameter mismatch on the relative efficiency and light output vs heterojunction diode current is illustrated in Fig. 26 for $\text{In}_x\text{Ga}_{1-x}\text{P}/\text{GaAs}$ double heterojunctions. Two sets of diodes were made (with n-type GaAs in the recombination region in each case), but with different In/Ga ratios so as to change the lattice parameter mismatch at the heterojunction. In the case where the interfacial lattice parameter is more nominally matched at the growth temperature by using $x = 0.485$, the L vs I curve is reasonably linear above 40 mA. However, where the lattice mismatch is severe (0.6%), the diode efficiency is an order of magnitude lower, and the L vs I relationship is steeper, indicating that more of the current is nonradiative even at high current densities, because of the high defect density.

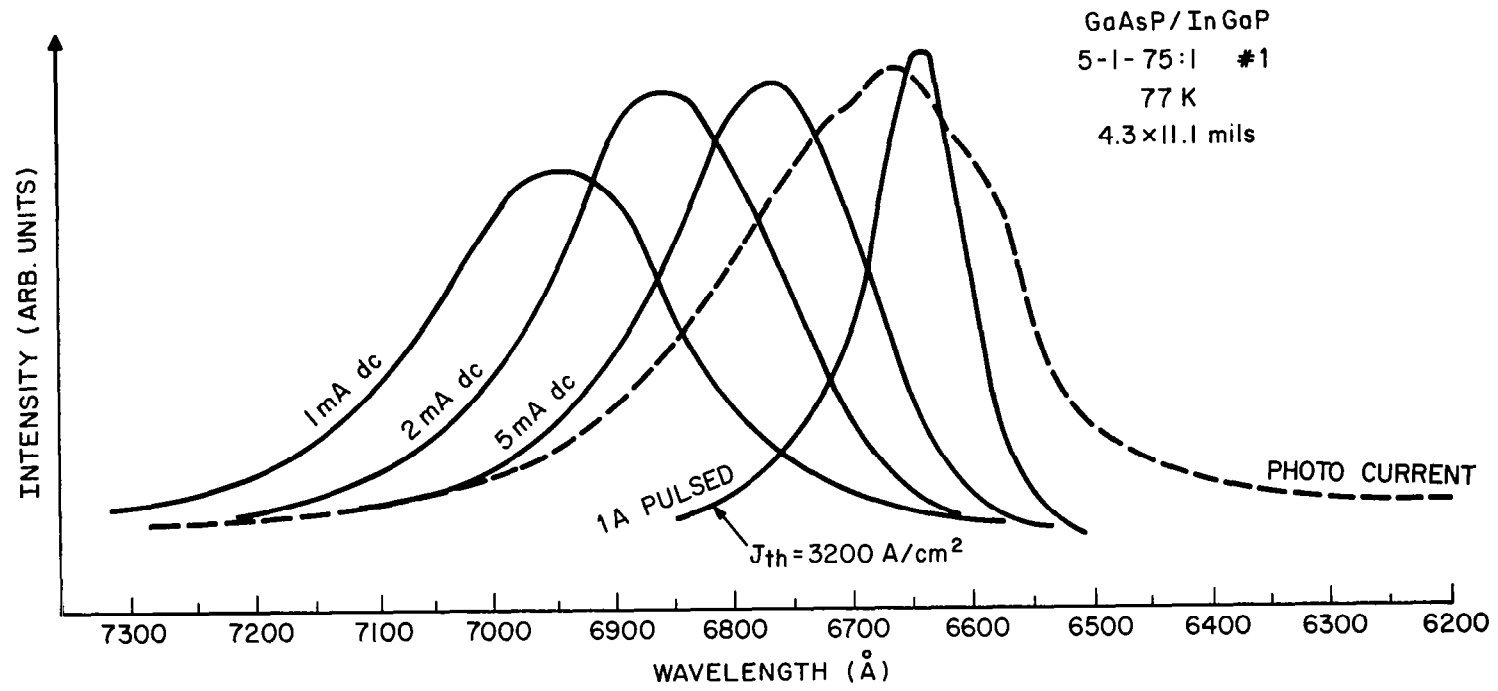


Figure 24. Shift of emission lines as a function of current as lasing is approached at 77 K.

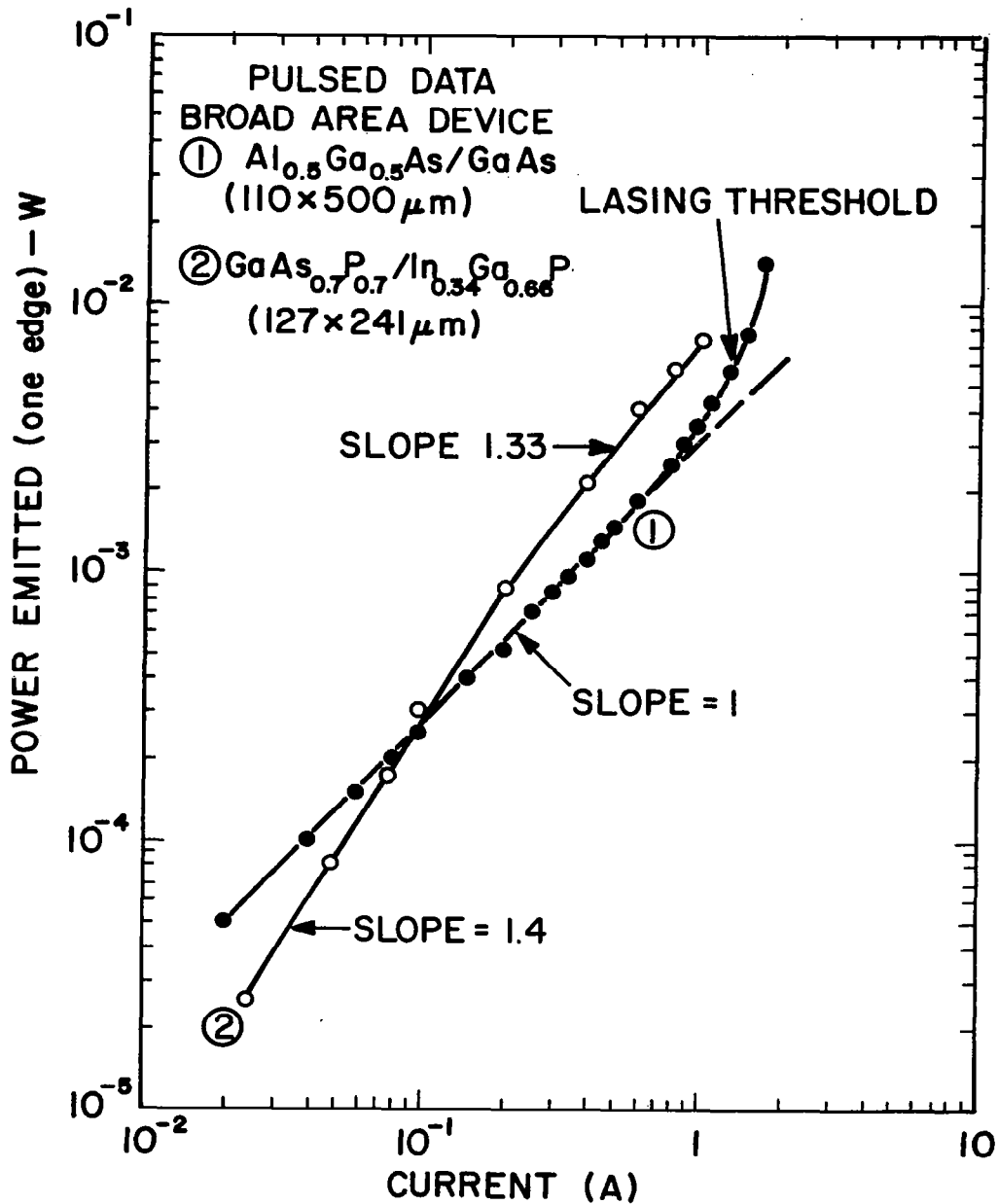


Figure 25. Light output as a function of the diode current of a GaAsP/InGaP heterojunction diode and of an (AlGa)As/GaAs DH device. The nonlinearity of the diode indicates the presence of strong nonradiative current components due to defects in the GaAsP/InGaP diode.

IV. RELIABILITY STUDIES

The use of zinc instead of germanium in the (AlGa)As bounding regions of the laser has been evaluated since this may affect the reliability of the device. At this time, no evidence has come to light indicating that the process *per se* is troublesome. Figure 27 shows the power curve of such a laser operating at a fixed heat sink temperature of 22°C for 1500 h. The power output is seen to have actually increased somewhat at fixed current because of the small reduction in I_{th} . The effect of possibly accelerating the degradation using higher heat sink temperature was attempted with a 40°C operating temperature. After 500 h of operation, no significant degradation has been noted for a laser emitting at 7650 Å.

The use of Al_2O_3 facet coatings to protect the lasers against facet damage has become standard in our laboratory (see Appendix A). An interesting example of the beneficial effects of the coatings is evident from Fig. 28 which shows the facet of a laser which was accidentally not fully passivated. Note that the uncoated regions of the laser show clear evidence of facet damage while the coated region near the center is damage-free.

With regard to long-term operating tests, a group of lasers with conventional technology has now passed 10,000 h (with facet coating) with less than 20% power reduction at constant current. Unpassivated lasers have shown some degradation when operated for periods of time in excess of 14,000 h. Figure 29 shows the power vs current curve (cw) in the course of operation spanning 14,000 h of a laser with a 100- μ m-wide stripe. The threshold current has increased from 0.7 to 0.8 A, with some reduction in the differential quantum efficiency. The laser has been operated for the past 5000 h at 0.9 A. Previously it was operated at 0.8 A.

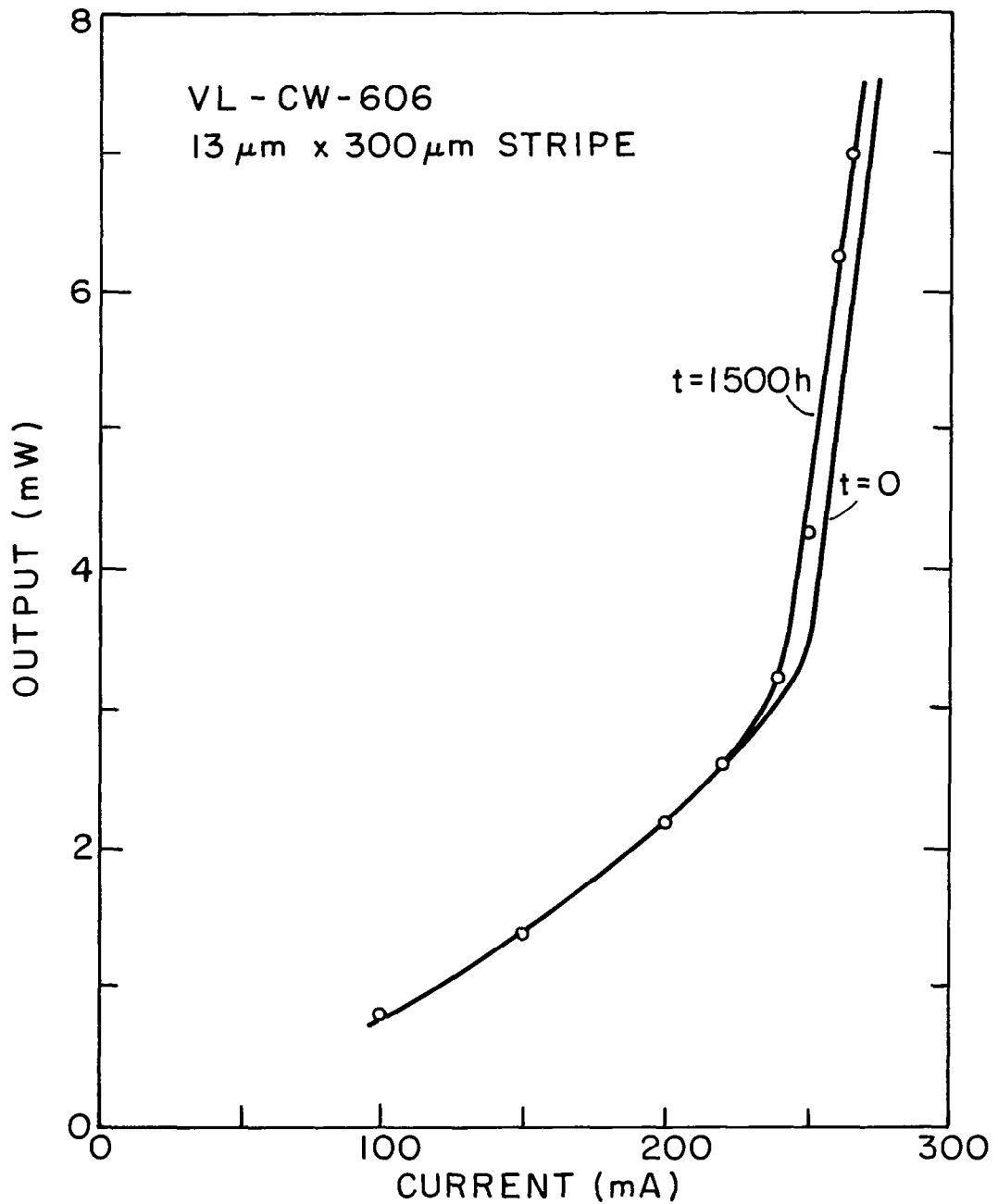


Figure 27. Power output as a function of current (cw) of a 13- μm -wide stripe laser made using the fast-cool Zn-doped process, before and after constant current operation.

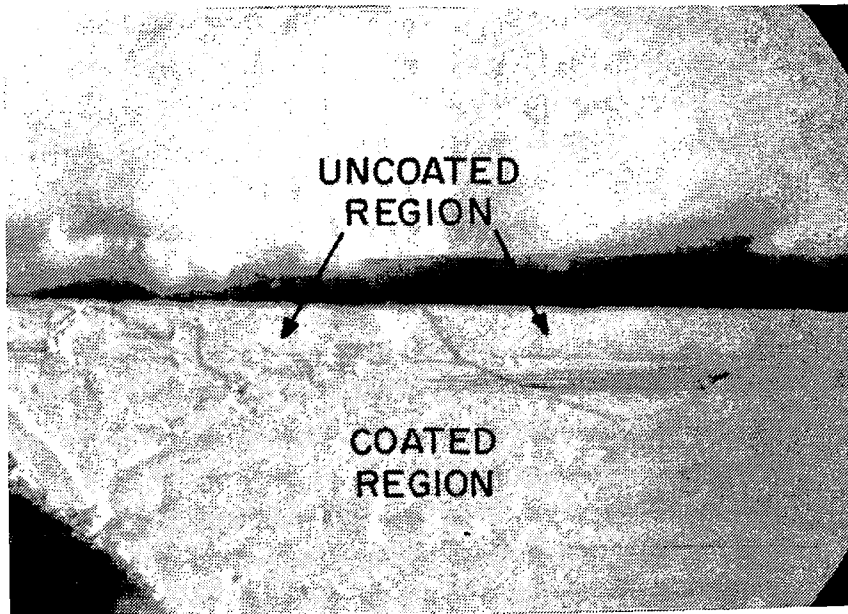


Figure 28. Laser facet following catastrophic degradation. Only the uncoated regions show facet damage, while the coated central region shows no evidence of such damage.

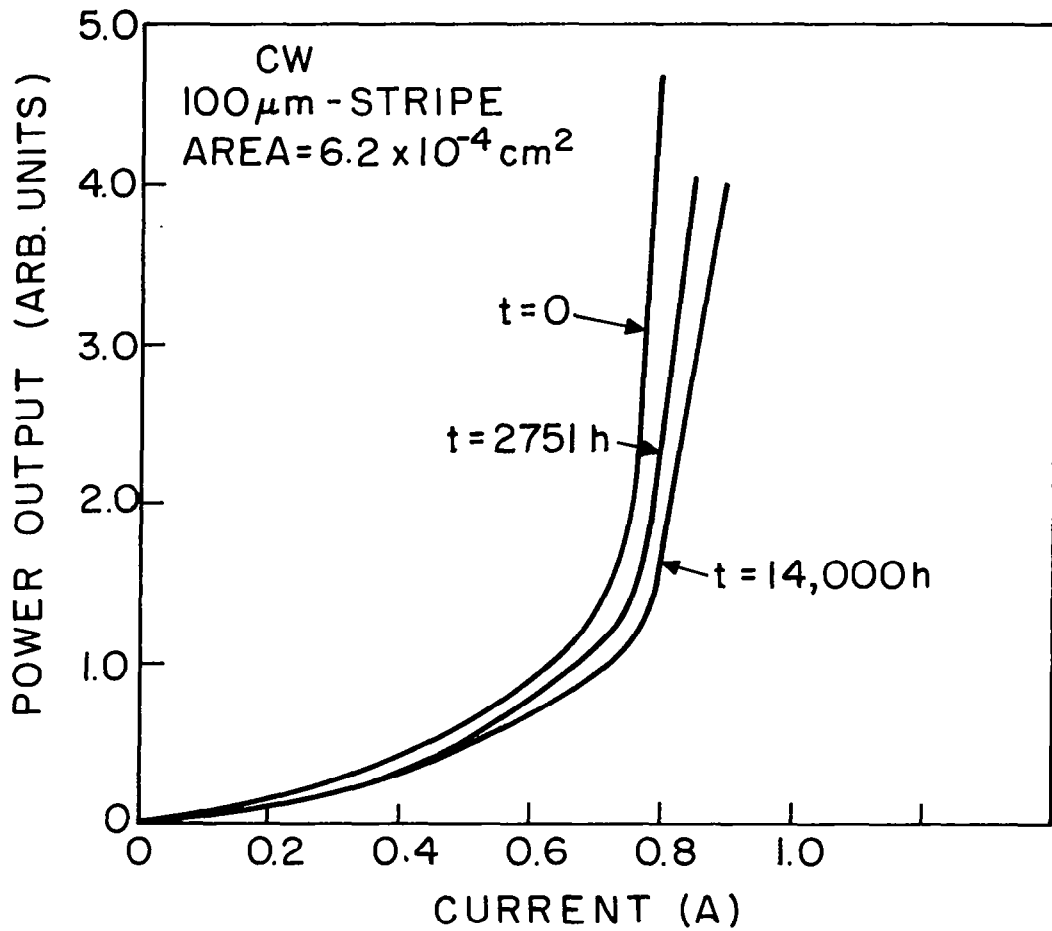


Figure 29. Power output as a function of current (cw) of a wide stripe laser during operation. For the first 9000 h, the laser was operated at 0.8 A; after that at 0.9 A.

V. CONCLUSIONS

The work reported here has demonstrated that laser diodes can be made in the visible portion of the spectrum with room-temperature threshold current densities equal in magnitude to values only recently achieved in the infrared. The (AlGa)As technology has been shown to lend itself to the fabrication of lasers at $\lambda = 7240 \text{ \AA}$ with $J_{\text{th}} = 2230 \text{ A/cm}^2$, a record low value well within the theoretical limits of room-temperature cw operation. A number of complex technological factors were overcome to accomplish this result, including the control of the appropriate dopant concentration in the passive regions of the device, and a rapid growth process to minimize cross-contamination of the layers in the growth apparatus. However, technological problems still remain at the short wavelength range of the alloy system, including control of the thermal resistance of the devices which, to date, has limited room-temperature cw operation to $\lambda = 7400 \text{ \AA}$ or longer. This result represents the first achievement of room-temperature cw operation in a range convenient for eye visibility. However, we believe that shorter wavelength room-temperature cw operation is possible with further technological progress.

A comparison of the experimental and theoretical laser data shows that the general trend of increasing threshold with decreasing internal quantum efficiency is followed. However, some anomalies are observed attributed to defects in the material. There is some evidence from applied stress measurements that these may be related to stresses in the diodes. Nevertheless, judging from the low threshold values achieved with our latest growth methods, it appears that much progress has been made in eliminating the detrimental effects of the internal diode stress.

Reliability tests conducted with our (AlGa)As laser structures are encouraging. Using the facet passivation process discussed in preliminary form in Appendix A, we have achieved 10,000 h to date of essentially

stable laser operation at *constant current* (less than 20% reduction in power output). Unpassivated structures with very large stripe widths of 100 μm have now operated for more than 14,000 h with moderate degradation as a result of some facet erosion. Thus, we believe that the laser diode technology is well founded for useful systems application, even those requiring exceptional reliability.

Among the achievements of the program on a new alloy system heterojunction structure is the construction of the first laser diodes of GaAsP/InGaP. These emit below 7000 \AA at all temperatures to 300 K. Using vapor-phase epitaxy, a series of devices were fabricated in the vicinity of the lattice-matching composition. These LOC (large optical cavity) lasers operated to 273 K, being limited by the defects introduced by what is believed to be slight lattice parameter mismatch. With further work, we believe that much better laser diodes can be constructed using this technology.

APPENDIX A ^{**}

Reliability Aspects and Facet Damage in High-Power Emission from (AlGa)As CW Laser Diodes at Room Temperature*

H. Kressel and I. Ladany

RCA Laboratories, Princeton, N.J. 08540

Abstract—Factors are described that limit the optical power output from (AlGa)As laser diodes ($\lambda = 8100\text{--}8300 \text{ \AA}$) operating cw at room temperature with uncoated facets. Rapid laser "catastrophic" degradation due to facet damage (in contrast to "bulk" phenomena previously considered) has been found to occur as a result of excessive optical flux density at the facets. The diodes studied are capable of initial cw power emission values of 25 to 100 mW from one facet depending on their dimensions. Data are presented showing long-term constant-current operation at power levels below these maximum values. Preliminary data are also presented on devices utilizing dielectric facet coatings to minimize facet damage.

Introduction

Significant progress has been made in improving the operating lifetime of cw heterojunction laser diodes (and high radiance LED's) at room temperature. This has resulted from improved knowledge concerning the relevant device aspects affecting the formation of non-radiative centers¹⁻⁶ and external factors such as facet erosion resulting from ambient conditions.⁵ While attention has been paid to internal device effects, it has been generally assumed that the cw power emission levels were too low to result in rapid device degradation due

* This research was partially supported by NASA, Langley Research Center, Hampton, Virginia, under Contract NAS1-11421 and the Office of Naval Research, Arlington, Virginia, under Contract N00014-73-C-0335.

****Reprinted from RCA Review 36, 230 (1975).**

to facet damage ("catastrophic degradation")⁷ well known to occur in pulsed diode operation when the power density at the emitting facet reaches values in the MW/cm² range. For pulsed laser operation, it is experimentally found⁸ that the power level at which facet damage occurs decreases approximately with pulse length t as $t^{-1/2}$. Hence, it is reasonable to suppose that cw laser operation will induce damage at substantially lower levels than usually observed in pulsed diode operation.

The object of the present work was to explore the power density limits in practical cw laser diodes. We show by comparing cw and pulsed diode operation that facet failure (uncoated facets) occurs at significantly reduced levels in cw operation. In addition, long term cw operation tests were conducted with similar lasers at initial power emission levels which did not exceed $\frac{1}{3}$ the maximum value from a given diode. Many thousands of hours of relatively stable operation are obtained under conditions of constant current operation.

Experimental Results

The diodes studied, designed for emission in the 8100–8300 Å spectral range, were Al_xGa_{1-x}As–Al_yGa_{1-y}As double heterojunction structures, with typically $x \approx 0.1$ in the recombination region and $y \approx 0.3$ in the adjoining p- and n-type regions, as discussed previously.⁵ The material was grown on (100) GaAs substrates by liquid-phase epitaxy using the thin-melt technique⁹ in a horizontal growth apparatus. The width of the n-type recombination region was 0.2–0.3 μm. Germanium was used to dope the p-type regions, while Sn or Te were used for the n-type regions. The recombination region was not deliberately doped, and has an electron concentration of 5×10^{16} cm⁻³. To minimize the thermal and electrical resistance of the diodes, the distance between the recombination region and the surface of the diode was typically 2–3 μm and included a highly doped p-type GaAs layer to improve the ohmic contact.

The combination of a very narrow recombination region and appropriate Al concentrations in the two surrounding layers of the diodes completely confines the carriers to the recombination region, but only partially confines the radiation there.¹⁰ This is reflected in the far-field radiation pattern, which shows a full beam width value (at half-power) of 33 to 38° in the direction perpendicular to the junction plane, indicative of an "effective aperture" greater than the recombination region width.

The active diode area was defined by a SiO₂-isolation stripe-contact process¹¹ with stripe widths of 13, 50, and 100 μm. The diodes

were mounted p-side down on copper heat sinks using indium as the solder.

Fig. 1 shows the current dependence of the light emitted by typical wide stripe diodes used in this study. For the 50 μm stripe width, the indicated threshold current is 0.76 A and the cw power output peaks at 90 mW (one side) at a current of 1.3 A. The saturation in the power output is due to the increase with current of the junction temperature and the consequent increase in the threshold current density. The position of the maximum in the power output depends on the thermal and electrical resistance of the diode, and on the threshold cur-

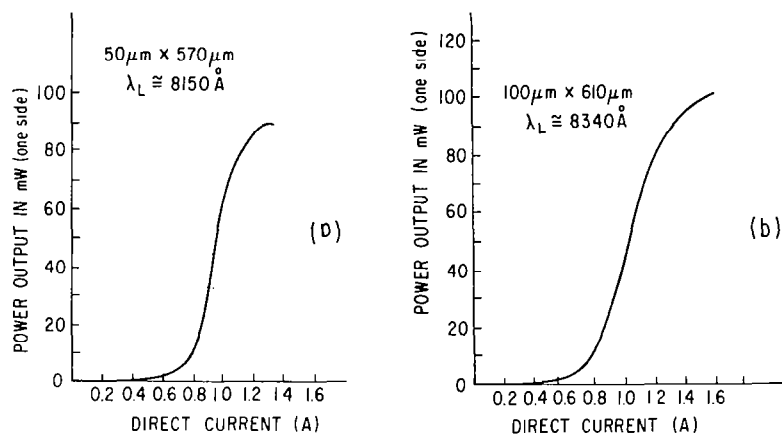


Fig. 1—Power emission from one laser facet as a function of direct current for two lasers selected from different wafers operating cw at room temperature: (a) diode with 50- μm -wide stripe contact; (b) diode with 100- μm -wide stripe contact.

rent density dependence on temperature.¹² Comparative studies were conducted with the 100- μm -wide stripe diodes in which the power output saturates at ~ 100 mW (~ 200 mW total emission) at a current of 1.6 A as shown in Fig. 1(b).

The facet damage effects were studied in the 13- and 50- μm -wide stripe diodes where cw-operation damage could be induced within relatively short periods of time (on the order 1 hr) when the diodes were operated at their peak optical output. The diode facets were uncoated and the damage experiments were conducted in a normal laboratory ambient with the heat sink temperature kept constant at $\sim 20^\circ\text{C}$, with provisions made to ensure that the diode facets were dry.

First, we consider facet damage seen in a 50- μm -wide stripe laser initially emitting 90 mW from one facet. When the emitted power had decreased to $\frac{1}{4}$ of its initial value, the damaged region on the facet shown in Fig. 2 was observed. This region is 25 μm wide and occurs in the central region under the stripe contact where the current and, hence, the power emission is at a maximum. (Two other samples

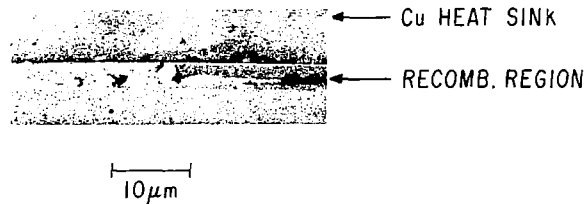


Fig. 2—Optical micrograph of the facet damage following operation at the 90 mW emission level from a 50- μm -wide stripe diode. The extent of the damaged region is $\sim 25 \mu\text{m}$ in the central region of the stripe width.

tested failed at power levels within 10 mW of the above value.) Facet damage could not be induced under similar test conditions in less efficient diodes operating at the same current of 1.3 A (for example, diodes emitting only 70 mW instead of 90 mW), suggesting a correlation between facet damage and the power emission level. Other observations were consistent with this hypothesis. No facet damage was induced in the 100- μm -wide stripe diodes where a power level as high as 110 mW was emitted from a region about twice as wide.

In the 13- μm -wide diodes, facet damage occurred at power levels between 23 and 35 mW (in four samples tested). As shown in Fig. 3, the damaged region extends over a width of 5–6 μm in the plane of the junction and is thus similar in this respect to the damage in the wider diodes, which extends over only part of the stripe. Consistent with the damage observed, the central portion of the stripe contact has the highest optical power density as shown by examination of the near-field emission of Fig. 4.* Note in the scanning-electron-micrograph of Fig. 3(b), that the mechanical damage spreads substantially beyond the recombination region in a direction *normal* to the junction plane.

In order to obtain a further basis of comparison, 13- μm -wide stripe diodes similar to those studied above were operated with pulse lengths of $\sim 100 \text{ nsec}^\dagger$ (1 kHz) and 400 nsec (250 Hz) under conditions

* We are indebted to H. S. Sommers, Jr. for these data.

† Gaussian pulse shape, 100 nsec width at half-intensity point.

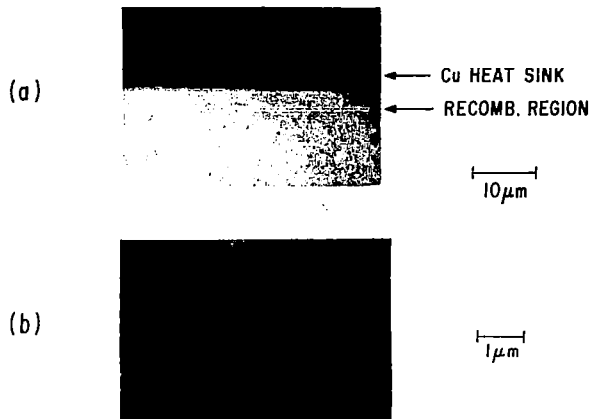


Fig. 3—Facet damage in a 13- μm -wide stripe diode: (a) optical micrograph showing damage extending over a distance of 5–6 μm in the stripe center; (b) scanning-electron-microscope micrograph showing that the damaged region extends substantially in the direction perpendicular to the junction plane.

to induce catastrophic damage. We found that of three diodes tested, the damage limits were 220, 230, and 260 mW with 100 nsec pulse length, while with the 400 nsec pulse, damages occurred at an average value of 90 mW. These damage power level values are therefore significantly greater than those found under cw operation.

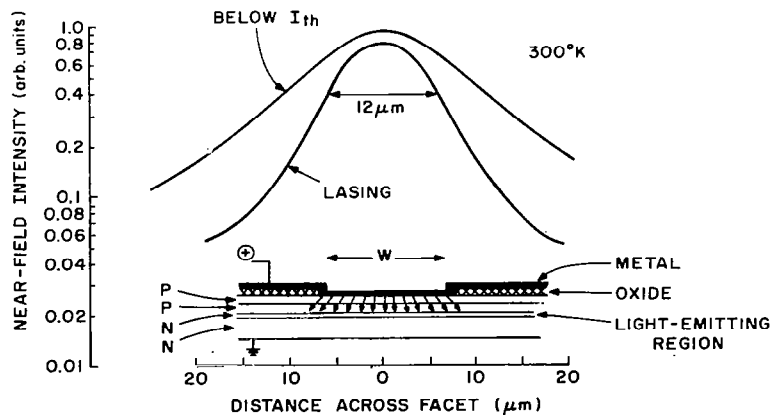


Fig. 4—Near-field intensity distribution of a 13- μm -wide stripe laser diode below and just above lasing threshold. Note the peak intensity at the center of the stripe region. (The two curves are shifted for convenience.)

The damage results described above are phenomena that occur in a relatively short time period. It is obviously of practical interest to determine the power level that can be sustained for long term operation, although a definitive study of such effects must involve a large number of samples and testing over periods of years. Preliminary tests were conducted with the diodes operating in a dry air atmosphere to minimize facet erosion accelerated by moisture.⁵ Both 13-

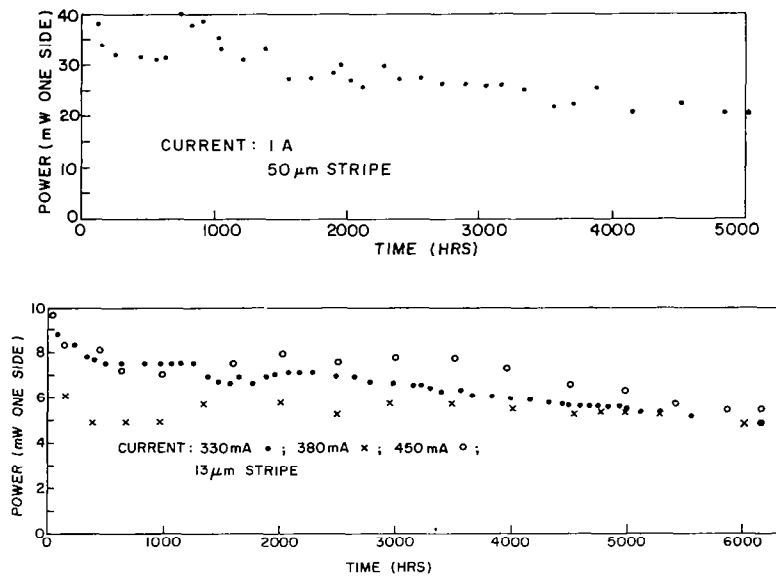


Fig. 5—Power emitted from one facet of cw (AlGa)As lasers operating at room temperature at constant current: (a) diode with 50- μm -wide stripe operating at a drive current of 1 A; (b) diodes with 13- μm -wide stripe operating at 330 mA, 380 mA, and 450 mA. The fluctuations in the power output are partially due to slight changes in the ambient temperature, which reversibly changes the threshold current density. (Uncoated laser facets.)

μm -wide stripe lasers and 50- μm -wide lasers were subjected to extended constant-current life tests at initial power levels not in excess of one-third the initial maximum attainable from a given device. The output from one facet as a function of operating time at a fixed current is shown in Fig. 5. The 50- μm -wide stripe diode is emitting between 22 and 33 mW from one facet for more than 5000 hrs with a drive current of 1 A. The 13- μm -wide lasers are emitting between 5 and 7 mW for more than 6000 hrs. (The fluctuations in the power

output seen in Fig. 5 are due to slight changes in the ambient temperature, which affect the threshold current and are reversible.) The power reduction seen in some of the diodes can be partly recovered by an increase in the diode current.

Discussion

It is evident that the damage level will scale with the extent of the emitting region, but the relationship between the observed power level for facet damage and the actual optical flux density is difficult to establish with high accuracy in stripe-contact diodes because of the graded lateral and perpendicular radiation distribution. For the 13- μm stripe diodes, the near-field pattern shows that the half-power point is reached at the edge of the stripe (Fig. 4), with the radiation being most intense in the central region where the damage is observed. However, stimulated emission occurs over a significant distance beyond the stripe width because of the lack of effective lateral current confinement. Considering the initial near-field distribution and power range at which damage was observed (23–35 mW), the power level in the 6 μm damaged region is estimated to be between 2 and 3 mW/ μm of emitting region.

For the 50 μm -wide stripes, we noted that the damage occurred in the central 25 μm of the device. We also noted that the power reduction was typically about 75% when damage of the type shown in Fig. 2 was observed. Taking the value of 90 mW at the damage point, the power concentrated in that 25 μm region can be assumed, as a first approximation, to represent 75% of 90 mW, or 68 mW, and hence to correspond to 2.7 mW/ μm of emitting region, a value within the above estimate for the 13- μm stripe diodes.

With regard to the power density, the best estimate of the effective perpendicular width of the emitting regions based on the far-field beam width of these devices (33–38°), is about 1 μm (but not less than 0.7 μm). Hence, the optical power density is $2 - 4.2 \times 10^5$ W/cm². These values can be compared to the much higher power level for facet damage estimated¹³ for 100-nsec pulse-length measurement of $4 - 8 \times 10^6$ W/cm². This large difference between the cw and 100-nsec-pulse-operated power densities for failure is also consistent with our measurement results for pulsed operation described above.

We wish to emphasize that in all cases of facet damage, the effect can occur at lower than expected power levels in the presence of dust particles on the laser facet, gross metallurgical flaws and, as pointed out earlier, when operation occurs in a relatively moist ambient.⁵ Facet protection is, therefore, very desirable. Furthermore, the use of

antireflective films (such as Al_2O_3 or SiO) on the facet are known to improve the catastrophic damage limit by as much as a factor of 3 in the case of pulsed diode operation.¹⁴ A similar improvement is expected for cw laser operation, and preliminary results do show a significant improvement in our cw devices.* The above results should not, therefore, be taken as indicative of the maximum power that can be reliably achieved from stripe-contact lasers having the indicated geometry.

Fig. 6 shows preliminary life data at constant current for a group of four 13- μm -wide stripe lasers with facet coatings. (The heat sink tem-

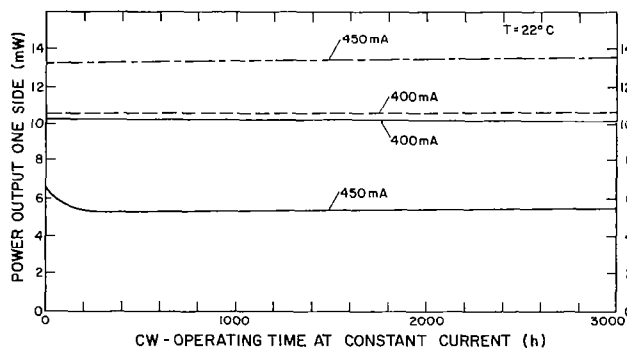


Fig. 6—Power emitted from one facet of four lasers with dielectric facet coating operating cw with a heat sink temperature of $22 \pm 1^\circ\text{C}$. The fixed current of operation is shown for each diode. The stripe width was 13 μm .

perature was maintained at $22^\circ\text{C} \pm 1^\circ$). Little or no evidence of degradation is seen in the time indicated. It is possible that the slow reduction in the power emission seen in the diodes with uncoated facets operating at constant current is due to facet damage, possibly starting at tiny flaws on the emitting facets.

It is encouraging to note that useful power output over many thousands of hours is possible with the relatively simple construction used for the present diodes. Long term operating-life data (in excess of 1000 hrs) were previously reported for diodes using other stripe contact formation techniques, including selective diffusion,³ etched mesas,⁶ and proton bombardment.² The reported data generally indicate that substantial current increases were needed to maintain rea-

* The dielectric coating experiments were performed in collaboration with M. Ettenberg and H. F. Lockwood.

sonably constant power output, an indication of degradation occurring in the course of operation.

Conclusions

A study has been made of operating conditions leading to facet damage (catastrophic degradation) of (AlGa)As laser diodes operating cw at room temperature (emission wavelength of 8100–8300 Å). It has been shown that facet damage occurs when the power level in the highest intensity region of the uncoated emitting facet reaches an estimated value of 2–3 mW/μm. Based on a reasonable approximation of the extent of emitting region in the direction perpendicular to the junction plane, the estimated optical power density is $2\text{--}4.2 \times 10^5$ W/cm². This value is several times lower than observed under short-pulse operation (100 nsec) for the same type of device.

It has also been shown that similar diodes have operated for periods of time in excess of 5000 hrs at initial power values that did not exceed $\frac{1}{3}$ the damage limit. The maximum reduction in the output of diodes with uncoated facets at constant current was below 50%. (An increase in the current can recover part of the power reduction.) The cause for the observed reduction in some of the diodes tested is as yet undetermined, but could be due to incipient facet damage originating at tiny facet flaws. Preliminary results using dielectric facet coating indicate that the damage limit is substantially increased (as has previously been observed in diodes designed for pulsed operation). Facet protection is believed to be important, for very long term stable operation, as a means of eliminating facet damage.

Acknowledgments

We are indebted to H. F. Lockwood and M. Ettenberg for collaboration on the dielectric film work; to D. P. Marinelli, V. M. Cannuli, D. B. Gilbert, H. Kowger, and M. Harvey for technical assistance; and E. R. Levin for the scanning electron microscopy.

References:

- ¹ A comprehensive discussion of the literature until 1973 was presented by H. Kressel and H. F. Lockwood, "A Review of Gradual Degradation Phenomena in Electroluminescent Diodes," *J. de Physique*, C3, Suppl. Vol. 35, p. 223, 1974.
- ² R. L. Hartman and R. W. Dixon, "Reliability of DH Lasers at Elevated Temperatures," *Appl. Phys. Lett.* **26**, p. 239, 1975, and references therein.
- ³ H. Yonezu, K. Kobayashi, K. Minemura, and I. Sakuma, "GaAs-Al_xGa_{1-x}As Double Heterostructure Laser for Optical Fiber Communication System," *International Electron Devices Meeting, IEEE, Tech. Digest*, p. 324, 1973.

- ⁴ M. Ettenberg, H. Kressel, and H. F. Lockwood, "Degradation of $\text{Al}_x\text{Ga}_{1-x}\text{As}$ Heterojunction Electroluminescent Devices," *Appl. Phys. Lett.*, **25**, p. 82, 1974.
- ⁵ I. Ladany and H. Kressel, "The Influence of Device Fabrication Parameters on the Gradual Degradation of $(\text{AlGa})\text{As}$ CW Laser Diodes," *Appl. Phys. Lett.*, **25**, p. 708, 1974.
- ⁶ O. Nakada, N. Chinone, S. Nakamura, H. Nakashima, and R. Itoh, "Continuous Operation Over 2500 Hours of Double Heterostructure Laser Diodes with Output Powers More than 80 mW," *Japan, J. Appl. Phys.*, **13**, p. 1485, 1974. (By private communication, the authors have indicated 40mW/face emission powers.)
- ⁷ H. Kressel and H. P. Mierop, "Catastrophic Degradation in GaAs Injection Lasers," *J. Appl. Phys.*, **38**, p. 5419, 1967.
- ⁸ Extensive data are given by P. G. Ellseev, "Degradation of Injection Lasers," in *Semiconductor Light Emitters and Detectors*, A. Frova, ed., North-Holland Publishing Co., Amsterdam, 1973, p. 338. [*J. Luminescence*, Vol. 7, 1973].
- ⁹ H. F. Lockwood and M. Ettenberg, "Thin Solution Multiple Layer Epitaxy," *J. Crystal Growth*, **15**, p. 81, 1972.
- ¹⁰ H. Kressel, J. K. Butler, F. Z. Hawrylo, H. F. Lockwood, and M. Ettenberg, "Mode Guiding in Symmetrical $(\text{AlGa})\text{As}$ -GaAs Heterojunction Lasers with Very Narrow Active Regions," *RCA Review*, **32**, p. 393, 1971.
- ¹¹ J. C. Dymont, "Hermite-Gaussian Mode Pattern in GaAs Junction Lasers," *Appl. Phys. Lett.*, **10**, p. 84, 1967.
- ¹² R. W. Keyes, "Thermal Problems of the CW Injection Laser," *IBM J. Research and Develop.*, **15**, p. 401, 1971.
- ¹³ B. W. Hakkl and R. Nash, "Catastrophic Failure in GaAs Lasers," *J. Appl. Phys.*, **45**, p. 3907, 1974.
- ¹⁴ M. Ettenberg, H. S. Sommers, Jr., H. Kressel, and H. F. Lockwood, "Control of Facet Damage in GaAs Laser Diodes," *Appl. Phys. Lett.*, **18**, p. 571, 1971.

REFERENCES

1. I. Ladany and H. Kressel, NASA CR-2556, 1975.
2. G. D. Pitt and J. Lees, Phys. Rev. B2, 4144 (1970).
3. O. Berolo and J. C. Wooley, Canad. J. Phys. 49, 1335 (1971).
4. H. Kressel and H. F. Lockwood, Appl. Phys. Letters 20, 175 (1972).
5. H. C. Casey, Jr., D. D. Sell, and M. B. Panish, Appl. Phys. Letters 24, 63 (1974).
6. H. Kressel, H. F. Lockwood, and J. K. Butler, J. Appl. Phys. 44, 4095 (1973).
7. F. Stern, IEEE J. Quant. Electron. QE-9, 290 (1973).
8. E. Pinkas, B. I. Miller, I. Hayashi, and P. W. Foy, IEEE J. Quant. Electron. QE-9, 281 (1973).
9. M. Ettenberg, Appl. Phys. Letters 27, 652 (1975).
10. P. Maruska and J. I. Pankove, Solid State Electronics 10, 917 (1967).
11. D. L. Rode, J. Appl. Phys. 45, 3887 (1974).
12. W. P. Dumke, Solid State Electronics 16, 1279 (1973).
13. M. Ettenberg and R. J. Paff, J. Appl. Phys. 41, 3926 (1970).
14. H. Kressel and F. Z. Hawrylo, Appl. Phys. Letters 17, 169 (1970).
15. B. I. Miller et al., Appl. Phys. Letters 18, 403 (1971).
16. Zh. I. Alferov et al., Sov. Phys. - Semiconductors 6, 495 (1972).
17. K. Itoh, M. Inone, and I. Teramoto, IEEE J. Quant. Electron. QE-11, 421 (1975).
18. W. P. Dumke, IEEE J. Quant. Electron. QE-11, 400 (1975).
19. J. Feinleib, S. Grove, W. Paul, and R. Zaller, Phys. Rev. 131, 2070 (1963).
20. T. Kobayashi and K. Sugiyama, Japan. J. Appl. Phys. 12, 1388 (1973).
21. C. J. Nuese, M. Ettenberg, and G. H. Olsen, Appl. Phys. Letters 25, 612 (1974).
22. C. J. Nuese and G. H. Olsen, Appl. Phys. Letters 26, 528 (1975).
23. V. S. Ban and M. Ettenberg, J. Chem. Phys. Solids 34, 1119 (1973).